Computer Physics Communications 280 (2022) 108477

Contents lists available at ScienceDirect

Computer Physics Communications

www.elsevier.com/locate/cpc

Chebyshev kernel polynomial method for efficient calculation of the quasiparticle random phase approximation response function ☆

A. Bjelčić [a], T. Nikšić [a,*], Z. Drmač [b]

[a] Department of Physics, Faculty of Science, University of Zagreb, Croatia
[b] Department of Mathematics, Faculty of Science, University of Zagreb, Croatia

ARTICLE INFO

Article history:
Received 9 November 2021
Received in revised form 7 July 2022
Accepted 24 July 2022
Available online 29 July 2022

Keywords:
Quasiparticle random phase approximation
Finite amplitude method
Chebyshev polynomials
Kernel polynomial method

ABSTRACT

Efficient and accurate algorithms for the calculation of the multipole response of deformed atomic nuclei are very important tools in nuclear structure, especially for large scale calculations. In this paper we present an implementation of the algorithm based on the expansion of the response function in terms of the Chebyshev polynomials in conjunction with the kernel polynomial method for a very efficient calculation of the quasiparticle random phase approximation response function. Several test calculations are performed in order to asses the applicability and feasibility of this algorithm, already used successfully in the field of computational solid state physics, in various nuclear structure calculations.

1. Introduction

Nuclear energy density functional framework provides an accurate description of ground-state properties and collective excitations of atomic nuclei, from relatively light systems to superheavy nuclei, and from the valley of β-stability to the particle drip-lines [1–4]. An important topic for this line of research are studies of multipole response in nuclei far from stability with possible occurrence of exotic modes of excitation [5,6]. Theoretical studies of the collective vibrations in heavy nuclei are nowadays performed routinely within the framework of the quasiparticle random phase approximation [7,8] (QRPA). Since the computational cost of the matrix implementation of the QRPA increases rapidly for deformed heavy nuclei, a finite amplitude method [9] (FAM) for solving the QRPA problem was developed and successfully applied in a number of studies [10–19]. Here we would like to take a step further and propose an implementation of the algorithm based on the expansion of the response function in terms of the Chebyshev polynomials in conjunction with the kernel polynomial method (KPM) for a very efficient calculation of the QRPA response function over a very broad energy range which could be very useful for large scale calculations. Kernel polynomial method originally developed in solid state physics [20] has been successfully used for calculating the Green's functions of a superconductor [21] and recently for controllable reconstruction of the spectral density in a strongly correlated many-body systems [22].

The paper is organized as follows. In section 2 we briefly recapitulate the quasiparticle random phase approximation and formally state the problem we would like to solve. Section 3 includes detailed description of the implementation of the Chebyshev kernel polynomial method for efficient calculation of the quasiparticle random phase approximation response function. In Section 4 we provide several test calculations to illustrate the feasibility and performance of the proposed method. Short summary is provided in section 5 and further mathematical details can be found in appendices.

2. Quasiparticle random phase approximation

In this section, we recapitulate the basic formulation and properties of the quasiparticle random phase approximation (QRPA) as a small amplitude limit of the time-dependent Hartree-Fock-Bogoliubov theory. For more details we refer the reader to Ref. [7]. Our starting point is the energy density functional $\mathcal{E}[\rho, \kappa, \kappa^*]$ which depends on the density matrix and pairing tensor:

$$\rho_{kl} = \langle\Phi|\hat{c}_l^\dagger \hat{c}_k|\Phi\rangle\,, \qquad \kappa_{kl} = \langle\Phi|\hat{c}_l \hat{c}_k|\Phi\rangle\,. \tag{1}$$

$|\Phi\rangle$ denotes the HFB vacuum and the operators $(\hat{c}_l^\dagger, \hat{c}_l)$ belong to the particle basis. Indices k and l in Eq. (1) denote the states in the adopted basis, e.g. the harmonic oscillator basis. The single-particle Hamiltonian h and the pairing field Δ are calculated as

☆ The review of this paper was arranged by Prof. Z. Was.

* Corresponding author.
E-mail address: tniksic@phy.hr (T. Nikšić).

https://doi.org/10.1016/j.cpc.2022.108477
0010-4655/

a variation of the energy density functional $\mathcal{E}$ with respect to the density matrix ρ and the pairing tensor κ^*, respectively:

$$h_{kl}[\rho,\kappa,\kappa^*] = \frac{\partial \mathcal{E}}{\partial \rho_{kl}}, \qquad \Delta_{kl}[\rho,\kappa,\kappa^*] = \frac{\partial \mathcal{E}}{\partial \kappa^*_{kl}}. \tag{2}$$

The particle operators $\hat{c}_l^\dagger, \hat{c}_l$ are connected to the quasi-particle operators $\hat{\alpha}_\mu^\dagger, \hat{\alpha}_\mu$ by the Bogoliubov transformation:

$$\hat{\alpha}_\mu^\dagger = \sum_l \left(U_{l\mu} \hat{c}_l^\dagger + V_{l\mu} \hat{c}_l \right). \tag{3}$$

The columns μ of the Bogoliubov matrices U and V are obtained by solving the HFB equation:

$$\begin{bmatrix} h - \lambda \mathbf{I} & \Delta \\ -\Delta^* & -h^* + \lambda \mathbf{I} \end{bmatrix} \begin{bmatrix} U_\mu \\ V_\mu \end{bmatrix} = E_\mu \begin{bmatrix} U_\mu \\ V_\mu \end{bmatrix}. \tag{4}$$

E_μ are the quasiparticle energies, and the chemical potential λ is determined by the particle number subsidiary condition.

Next, we assume that the nucleus is subjected to a weak external field of a given frequency:

$$\hat{F}(t) = \eta \left(\hat{F}(\omega) e^{-\mathrm{i}\omega t} + \hat{F}^\dagger(\omega) e^{+\mathrm{i}\omega t} \right), \tag{5}$$

where η denotes small real parameter. In the quasiparticle basis $\hat{F}(\omega)$ reads:

$$\hat{F}(\omega) = \frac{1}{2} \sum_{\mu\nu} \left(F^{20}_{\mu\nu}(\omega) \hat{\alpha}_\mu^\dagger \hat{\alpha}_\nu^\dagger + F^{02}_{\mu\nu}(\omega) \hat{\alpha}_\nu \hat{\alpha}_\mu \right) + \sum_{\mu\nu} F^{11}_{\mu\nu}(\omega) \hat{\alpha}_\mu^\dagger \hat{\alpha}_\nu. \tag{6}$$

We notice that the second summation in Eq. (6) does not contribute in the linear approximation. The Bogoliubov transformation of the external field, i.e. explicit expressions for the matrices $F^{20}_{\mu\nu}(\omega)$ and $F^{02}_{\mu\nu}(\omega)$, can be found in Ref. [7]. The time evolution of the quasiparticle operators is governed by the time-dependent Hartree-Fock Bogoliubov equation (TDHFB):

$$\mathrm{i}\partial_t \hat{\alpha}_\mu(t) = \left[\hat{H}(t) + \hat{F}(t), \hat{\alpha}_\mu(t) \right], \tag{7}$$

with:

$$\hat{\alpha}_\mu(t) = \left(\hat{\alpha}_\mu + \delta\hat{\alpha}_\mu(t) \right) e^{\mathrm{i}E_\mu t}, \tag{8}$$

$$\delta\hat{\alpha}_\mu(t) = \eta \sum_\nu \hat{\alpha}_\nu^\dagger \left(X_{\nu\mu}(\omega) e^{-\mathrm{i}\omega t} + Y^*_{\nu\mu}(\omega) e^{+\mathrm{i}\omega t} \right), \tag{9}$$

where E_μ is the quasiparticle energy introduced in Eq. (4). $X_{\mu\nu}(\omega)$ and $Y_{\mu\nu}(\omega)$ denote the QRPA forward and backward amplitudes, respectively. The external field $\hat{F}(t)$ induces oscillations of the density and pairing tensor around the ground state values with the same perturbation frequency ω and these in turn produce the induced fields in the single-particle Hamiltonian and pairing field. Finally, the HFB Hamiltonian can also be decomposed into the ground-state and oscillating part.

The $X(\omega)$ and $Y(\omega)$ amplitudes are calculated by solving the linear response equation:

$$\left(\begin{bmatrix} A & B \\ B^* & A^* \end{bmatrix} - \omega \begin{bmatrix} \mathbf{I} & \mathbf{0} \\ \mathbf{0} & -\mathbf{I} \end{bmatrix} \right) \begin{bmatrix} X(\omega) \\ Y(\omega) \end{bmatrix} = - \begin{bmatrix} F^{20}(\omega) \\ F^{02}(\omega) \end{bmatrix}, \tag{10}$$

where $X(\omega), Y(\omega), F^{20}(\omega), F^{02}(\omega)$ are the corresponding vectorized matrices. Furthermore, the left-hand side of Eq. (10) leads to the QRPA eigenvalue equation when the right-hand side is set to zero:

$$\begin{bmatrix} A & B \\ B^* & A^* \end{bmatrix} \begin{bmatrix} X^i \\ Y^i \end{bmatrix} = \Omega_i \begin{bmatrix} \mathbf{I} & \mathbf{0} \\ \mathbf{0} & -\mathbf{I} \end{bmatrix} \begin{bmatrix} X^i \\ Y^i \end{bmatrix}. \tag{11}$$

The QRPA matrices A and B are calculated from second variational derivative of the energy density functional $\mathcal{E}$ with respect to the density matrix and pairing tensor. The matrix formulation of the QRPA problem becomes computationally very demanding, especially for applications to deformed atomic nuclei. The reason is the large number of quasiparticle states involved in the calculations which makes the dimension of the QRPA matrix rather large. This means that one first has to calculate large number of matrix elements and subsequently diagonalize huge QRPA matrix. Since neither of these two tasks is feasible in large-scale calculations involving deformed nuclei, a number of efficient methods to solve the QRPA problem have been formulated [23,24]. Among them the finite-amplitude method (FAM), first proposed in Ref. [9], has proved very successful in numerous applications [10–19]. Within the framework of the finite-amplitude method, one can avoid explicit construction and diagonalization of the QRPA matrix and instead iteratively solve the linear response problem:

$$\left(E_\mu + E_\nu - \omega \right) X_{\mu\nu}(\omega) + \delta H^{20}_{\mu\nu}(\omega) = -F^{20}_{\mu\nu}(\omega), \tag{12}$$

$$\left(E_\mu + E_\nu + \omega \right) Y_{\mu\nu}(\omega) + \delta H^{02}_{\mu\nu}(\omega) = -F^{02}_{\mu\nu}(\omega). \tag{13}$$

$\delta H^{20}_{\mu\nu}(\omega)$ and $\delta H^{02}_{\mu\nu}(\omega)$ are the matrix elements of the induced HFB Hamiltonian in the quasiparticle basis. In principle, by expanding the $\delta H^{20}(\omega)$ and $\delta H^{02}(\omega)$ in terms of the amplitudes $X(\omega)$ and $Y(\omega)$, one could show that Eqs. (10) and (12)-(13) are equivalent. In order to avoid divergences at the positions of the QRPA poles Ω_i, the frequency in Eqs. (12)-(13) is set complex, i.e., $\omega \to \omega + \mathrm{i}\gamma$. Small imaginary part γ corresponds to the smearing width. By employing the $X(\omega)$ and $Y(\omega)$ amplitudes, we can calculate the response function:

$$\frac{dB(\hat{F},\omega)}{d\omega} = -\frac{1}{\pi} \operatorname{Im} S(\hat{F},\omega), \tag{14}$$

with strength function defined as:

$$S(\omega,\hat{F}) = \sum_{\mu<\nu} \left(F^{20}_{\mu\nu}(\omega)^* X_{\mu\nu}(\omega) + F^{02}_{\mu\nu}(\omega)^* Y_{\mu\nu}(\omega) \right). \tag{15}$$

For a more complete description of the finite amplitude method for solving the quasiparticle random phase approximation we refer the reader to Ref. [12] and references cited therein. Furthermore, in this work we will assume that the excitation operators $F^{20}_{\mu\nu}(\omega), F^{02}_{\mu\nu}(\omega)$ do not depend on the frequency ω, i.e. $F^{20}_{\mu\nu}(\omega) = F^{20}_{\mu\nu}$ and $F^{02}_{\mu\nu}(\omega) = F^{02}_{\mu\nu}$. In practical calculations this assumption is virtually always fulfilled.

2.1. Properties of the QRPA matrix

Before we formally state the problem, we would like to collect some well known technical results related to the properties of the QRPA matrices [8,7]. Regarding the notation, throughout the paper we use $A^\dagger$ for Hermitian conjugate matrix, A^T for transposed matrix and A^* for element-wise complex conjugate matrix of arbitrary matrix $A \in \mathbb{C}^{m\times n}$. We also use MATLAB notation for diagonal matrices, i.e. if $x \in \mathbb{C}^n$ is a vector, then $\mathrm{diag}[x] \in \mathbb{C}^{n\times n}$ is a diagonal matrix having elements of the vector x as diagonal elements, i.e. $\mathrm{diag}[x]_{i,j} = \delta_{i,j} x_i$, for $i, j = 1, \ldots, n$. If the QRPA matrix $\begin{bmatrix} A & B \\ B^* & A^* \end{bmatrix}$ is positive-definite, which corresponds to a minimum in the energy surface of the HFB solution, then there exist positive eigenfrequencies $\Omega_i > 0$ and QRPA amplitudes $X^i, Y^i \in \mathbb{C}^n$ which are the generalized eigenpair of the QRPA matrix:

$$\begin{bmatrix} A & B \\ B^* & A^* \end{bmatrix} \begin{bmatrix} X^i \\ Y^i \end{bmatrix} = \Omega_i \begin{bmatrix} X^i \\ -Y^i \end{bmatrix}, \tag{16}$$

with generalized normalization and closure relations:

$$\sum_{\mu=1}^{n} (X^i_\mu)^* X^j_\mu - (Y^i_\mu)^* Y^j_\mu = \delta_{i,j} \quad \text{and}$$
$$\sum_{i=1}^{n} X^i_\mu (X^i_\nu)^* - (Y^i_\mu)^* Y^i_\nu = \delta_{\mu,\nu}. \tag{17}$$

The detailed proof of the previous statement is included in the Appendix A as Proposition 1. Next, we give a straightforward but useful result related to the polynomial $P \in \mathbb{C}[x]$ with complex coefficients evaluated at a matrix: $\begin{bmatrix} \mathbf{I} & \mathbf{0} \\ \mathbf{0} & -\mathbf{I} \end{bmatrix} \begin{bmatrix} A & B \\ B^* & A^* \end{bmatrix}$.

Lemma 1. *Let* $\begin{bmatrix} A & B \\ B^* & A^* \end{bmatrix} \in \mathbb{C}^{2n\times 2n}$ *be a positive-definite QRPA matrix and* $X, Y \in \mathbb{C}^{n\times n}$ *QRPA amplitudes matrices. Furthermore, let* $\Omega \in \mathbb{R}^{n\times n}$ *be a diagonal matrix containing the QRPA eigenfrequencies. Then for any polynomial* $P \in \mathbb{C}[x]$ *the following equation holds:*

$$P\left(\begin{bmatrix} \mathbf{I} & \mathbf{0} \\ \mathbf{0} & -\mathbf{I} \end{bmatrix} \begin{bmatrix} A & B \\ B^* & A^* \end{bmatrix}\right) = \begin{bmatrix} X & Y^* \\ Y & X^* \end{bmatrix} \begin{bmatrix} P(+\Omega) & \mathbf{0} \\ \mathbf{0} & P(-\Omega) \end{bmatrix} \begin{bmatrix} X & Y^* \\ Y & X^* \end{bmatrix}^{-1}. \tag{18}$$

Proof. Equation (A.5) shows that the matrix $\begin{bmatrix} X & Y^* \\ Y & X^* \end{bmatrix}$ is invertible. Therefore, Eq. (A.4) can be written as:

$$\begin{bmatrix} \mathbf{I} & \mathbf{0} \\ \mathbf{0} & -\mathbf{I} \end{bmatrix} \begin{bmatrix} A & B \\ B^* & A^* \end{bmatrix} = \begin{bmatrix} X & Y^* \\ Y & X^* \end{bmatrix} \begin{bmatrix} +\Omega & \mathbf{0} \\ \mathbf{0} & -\Omega \end{bmatrix} \begin{bmatrix} X & Y^* \\ Y & X^* \end{bmatrix}^{-1}, \tag{19}$$

which immediately yields Eq. (18). □

Finally, we recall two elementary facts which will be useful.

Lemma 2. *Let* $A \in \mathbb{C}^{n\times n}$ *be a complex symmetric matrix, i.e.* $A^T = A$. *Then for any* $x \in \mathbb{C}^n$ *there holds:*

$$\operatorname{Im}\left[x^\dagger A x\right] = x^\dagger \operatorname{Im}[A] x. \tag{20}$$

Proof. Writing $A = A_r + A_i\mathrm{i}$, for $A_r, A_i \in \mathbb{R}^{n\times n}$ real symmetric and $x = x_r + x_i\mathrm{i}$ for $x_r, x_i \in \mathbb{R}^n$, one trivially sees:

$$\operatorname{Im}\left[x^\dagger A x\right] = x_r^T A_i x_r + x_i^T A_i x_i + x_r^T A_r x_i - x_i^T A_r x_r, \tag{21}$$
$$x^\dagger \operatorname{Im}[A] x = x^\dagger A_i x = x_r^T A_i x_r + x_i^T A_i x_i + \left(x_r^T A_i x_i - x_i^T A_i x_r\right)\mathrm{i}. \tag{22}$$

Since $A_r^T = A_r$ and $A_i^T = A_i$, there holds: $x_r^T A_r x_i = x_i^T A_r x_r$ and $x_r^T A_i x_i = x_i^T A_i x_r$, which yields Eq. (20). □

Lemma 3. *Let* $f : [-1, +1] \to \mathbb{R}$ *be continuous function,* $a > 0$ *and let* $\Omega \in \langle -a, +a \rangle$. *Then there holds:*

$$\lim_{\gamma\to 0^+} \int_{-a}^{+a} f(\omega/a) \frac{\gamma/\pi}{(\omega-\Omega)^2+\gamma^2} d\omega = f(\Omega/a). \tag{23}$$

Proof. Follows from a restricted version of $\delta(x) = \lim_{\gamma\to 0^+} \frac{\gamma/\pi}{x^2+\gamma^2}$ to $[-a, +a]$ domain. □

2.2. Problem statement

Next, we give a detailed description of the problem that we would like to solve in this paper. Suppose we have $A, B \in \mathbb{C}^{N_p\times N_p}$ satisfying $A^\dagger = A$, $B^T = B$, such that the QRPA matrix:

$$\begin{bmatrix} A & B \\ B^* & A^* \end{bmatrix} \in \mathbb{C}^{2N_p\times 2N_p}, \tag{24}$$

is positive-definite. Furthermore, let us suppose that two vectors $F^{20}, F^{02} \in \mathbb{C}^{Np}$ are given. For $\omega \in \mathbb{R}$ and $\gamma > 0$ we denote the complex frequency $\omega_\gamma = \omega + \gamma\mathrm{i}$ in the upper complex plane. Let the vectors $X(\omega_\gamma), Y(\omega_\gamma) \in \mathbb{C}^{N_p}$ be the solution of the following linear system:

$$\left(\begin{bmatrix} A & B \\ B^* & A^* \end{bmatrix} - \omega_\gamma \begin{bmatrix} \mathbf{I} & \mathbf{0} \\ \mathbf{0} & -\mathbf{I} \end{bmatrix}\right) \begin{bmatrix} X(\omega_\gamma) \\ Y(\omega_\gamma) \end{bmatrix} = -\begin{bmatrix} F^{20} \\ F^{02} \end{bmatrix}. \tag{25}$$

We define the strength function $S : \mathbb{R} + \mathbb{R}^+\mathrm{i} \to \mathbb{C}$ as:

$$S(\omega_\gamma) := \begin{bmatrix} F^{20} \\ F^{02} \end{bmatrix}^\dagger \begin{bmatrix} X(\omega_\gamma) \\ Y(\omega_\gamma) \end{bmatrix}. \tag{26}$$

Our task is to calculate the response function $\frac{dB}{d\omega} : \mathbb{R} \to \mathbb{R}$ defined as:

$$\frac{dB(\omega)}{d\omega} := \lim_{\gamma\to 0^+} \frac{-1}{\pi} \operatorname{Im}[S(\omega_\gamma)]. \tag{27}$$

First, we will show that the strength is well defined, i.e. that a matrix in Eq. (25) is invertible for any ω_γ. Later, it will be clear that the limit in Eq. (27) exists in the weak-* topology as a limit of sequence of distributions. According to the Proposition 1, there exist $X, Y \in \mathbb{C}^{N_p\times N_p}$ and $\Omega = \operatorname{diag}[\Omega_i]_{i=1}^{N_p} \in \mathbb{R}^{N_p\times N_p}$ such that $\Omega_i > 0$ for all $i = 1, \ldots, N_p$ and:

$$\begin{bmatrix} \mathbf{I} & \mathbf{0} \\ \mathbf{0} & -\mathbf{I} \end{bmatrix} \begin{bmatrix} A & B \\ B^* & A^* \end{bmatrix} = \begin{bmatrix} X & Y^* \\ Y & X^* \end{bmatrix} \begin{bmatrix} +\Omega & \mathbf{0} \\ \mathbf{0} & -\Omega \end{bmatrix} \begin{bmatrix} X & Y^* \\ Y & X^* \end{bmatrix}^{-1}, \tag{28}$$

$$\begin{bmatrix} X & Y^* \\ Y & X^* \end{bmatrix}^{-1} = \begin{bmatrix} \mathbf{I} & \mathbf{0} \\ \mathbf{0} & -\mathbf{I} \end{bmatrix} \begin{bmatrix} X & Y^* \\ Y & X^* \end{bmatrix}^\dagger \begin{bmatrix} \mathbf{I} & \mathbf{0} \\ \mathbf{0} & -\mathbf{I} \end{bmatrix}. \tag{29}$$

Thus, one can easily see that for any ω_γ in the upper complex plane, the matrix:

$$\begin{bmatrix} A & B \\ B^* & A^* \end{bmatrix} - \omega_\gamma \begin{bmatrix} \mathbf{I} & \mathbf{0} \\ \mathbf{0} & -\mathbf{I} \end{bmatrix} = \begin{bmatrix} \mathbf{I} & \mathbf{0} \\ \mathbf{0} & -\mathbf{I} \end{bmatrix} \begin{bmatrix} X & Y^* \\ Y & X^* \end{bmatrix} \times \times \begin{bmatrix} +\Omega - \omega_\gamma \mathbf{I} & \mathbf{0} \\ \mathbf{0} & -\Omega - \omega_\gamma \mathbf{I} \end{bmatrix} \begin{bmatrix} X & Y^* \\ Y & X^* \end{bmatrix}^{-1} \tag{30}$$

is invertible, rendering $S(\omega_\gamma)$ well defined with formula:

$$S(\omega_\gamma) = -\left(\begin{bmatrix} X & Y^* \\ Y & X^* \end{bmatrix}^\dagger \begin{bmatrix} F^{20} \\ F^{02} \end{bmatrix}\right)^\dagger \times \times \begin{bmatrix} (\Omega - \omega_\gamma \mathbf{I})^{-1} & \mathbf{0} \\ \mathbf{0} & (\Omega + \omega_\gamma \mathbf{I})^{-1} \end{bmatrix} \times \times \left(\begin{bmatrix} X & Y^* \\ Y & X^* \end{bmatrix}^\dagger \begin{bmatrix} F^{20} \\ F^{02} \end{bmatrix}\right). \tag{31}$$

According to Lemma 2, one immediately obtains:

$$-\frac{1}{\pi}\,\mathrm{Im}[S(\omega_\gamma)] = \left(\begin{bmatrix} X & Y^* \\ Y & X^* \end{bmatrix}^\dagger \begin{bmatrix} F^{20} \\ F^{02} \end{bmatrix}\right)^\dagger \times \times \begin{bmatrix} \frac{\gamma/\pi}{(\omega-\Omega)^2+\gamma^2} & \mathbf{0} \\ \mathbf{0} & \frac{-\gamma/\pi}{(\omega+\Omega)^2+\gamma^2} \end{bmatrix} \times \times \left(\begin{bmatrix} X & Y^* \\ Y & X^* \end{bmatrix}^\dagger \begin{bmatrix} F^{20} \\ F^{02} \end{bmatrix}\right), \tag{32}$$

where it is now clear that the limit of distributions in Eq. (27) exists, i.e. the response function $\frac{dB(\omega)}{d\omega}$ is well defined distribution on $\mathbb{R}$.

In direct implementations, the QRPA matrix is constructed explicitly and subsequently diagonalized by solving Eq. (28). The resulting matrices X, Y and Ω are used to calculate the strength according to Eq. (31) for arbitrary smearing parameter $\gamma > 0$. The main advantage of this approach is that one can use the calculated matrices X, Y and Ω to find the response for arbitrary excitation operator $\hat{F}$. This is analogous to solving the linear system of equations $\mathbf{A}x = b$, in the case when we know the spectral decomposition: $\mathbf{A} = \mathbf{S}\mathbf{\Lambda}\mathbf{S}^{-1}$. Then for any right-hand side vector b, one can easily find the solution: $x = \mathbf{S}\mathbf{\Lambda}^{-1}\mathbf{S}^{-1}b$. However, because this approach is computationally prohibitive for deformed atomic nuclei due to the large dimension of the QRPA matrix (24), in practice one often solves the system of linear equations (25) for preselected excitation operator $\hat{F}$ and smearing parameter $\gamma > 0$. In this case, one only obtains the shape profile $\left(\omega, S\left(\omega_\gamma\right)\right)$ of the strength function $S(\omega_\gamma)$, but for most applications this is quite satisfactory.

A very successful approach for solving the linear response problem is the finite amplitude method, described at the beginning of this section. When solving the linear system Eq. (25) for fixed frequency ω_γ, one usually uses an iterative solver which does not require the access to the full QRPA matrix, but rather only requires the access to the linear mapping:

$$\begin{bmatrix} x \\ y \end{bmatrix} \mapsto \begin{bmatrix} A & B \\ B^* & A^* \end{bmatrix}\begin{bmatrix} x \\ y \end{bmatrix}, \quad \text{for given} \quad x, y \in \mathbb{C}^{N_p}. \tag{33}$$

This mapping, equivalent to the FAM equations (12)-(13), can actually be constructed without explicit calculation of the residual nuclear interaction (i.e. without explicit construction of A and B matrices), which makes the FAM method convenient in practical implementations. Since the main goal of this paper is to improve the performance of the existing FAM solvers, we will only assume the access to the mapping (33). We will show that one can obtain an accurate approximation to the response function $\frac{dB(\omega)}{d\omega}$ in fewer number of FAM iterations. The proposed method is easy to implement in the existing FAM solvers with minimum additional effort.

3. Implementation of the kernel polynomial method for calculating the QRPA response function

3.1. Chebyshev expansion

First, we assume that all QRPA eigenfrequencies $(\pm\Omega_i)_{i=1}^{N_p}$ are contained in the finite interval $\langle -\Omega_b, +\Omega_b\rangle$. The parameter $\Omega_b > 0$ is referred to as the bounding frequency. Next, we fix the smearing parameter $\gamma > 0$, and since the set of Chebyshev polynomials:

$$T_n(x) = \cos(n \arccos(x)),\ x \in [-1, +1],\ n \in \mathbb{N}_0, \tag{34}$$

form an orthonormal basis, we expand the function $\frac{-1}{\pi}\mathrm{Im}[S(\omega_\gamma)]$ for $\omega \in \langle -\Omega_b, +\Omega_b\rangle$ as the following Chebyshev series:

$$\frac{-1}{\pi}\,\mathrm{Im}[S(\omega_\gamma)] = \frac{2/\pi}{\sqrt{\Omega_b^2-\omega^2}}\sum_{n=0}^{+\infty}\mu_n^{(\gamma)}T_n\left(\frac{\omega}{\Omega_b}\right), \tag{35}$$

where $\mu_n^{(\gamma)} \in \mathbb{R}$ are the expansion coefficients. Using the orthogonality of the Chebyshev polynomials:

$$\int_{-1}^{+1}\frac{T_n(x)T_m(x)}{\sqrt{1-x^2}}dx = \frac{\pi}{2}(1+\delta_{n,0})\delta_{m,n}, \quad m, n \in \mathbb{N}_0, \tag{36}$$

one easily obtains the formula for the expansion coefficients:

$$\mu_n^{(\gamma)} = \frac{1}{1+\delta_{n,0}}\int_{-\Omega_b}^{+\Omega_b}\frac{-1}{\pi}\,\mathrm{Im}[S(\omega_\gamma)]T_n\left(\frac{\omega}{\Omega_b}\right)d\omega. \tag{37}$$

From Eq. (32) and using (29) we easily see:

$$-\frac{1}{\pi}\,\mathrm{Im}[S(\omega_\gamma)] = \begin{bmatrix} F^{20} \\ F^{02} \end{bmatrix}^\dagger \begin{bmatrix} X & Y^* \\ Y & X^* \end{bmatrix} \times \times \begin{bmatrix} \frac{\gamma/\pi}{(\omega-\Omega)^2+\gamma^2} & \mathbf{0} \\ \mathbf{0} & \frac{\gamma/\pi}{(\omega+\Omega)^2+\gamma^2} \end{bmatrix} \times \times \begin{bmatrix} X & Y^* \\ Y & X^* \end{bmatrix}^{-1} \begin{bmatrix} F^{20} \\ -F^{02} \end{bmatrix}, \tag{38}$$

and thus, according to Lemma 3, the following equation holds:

$$\lim_{\gamma\to 0^+}\mu_n^{(\gamma)} = \frac{1}{1+\delta_{n,0}}\begin{bmatrix} F^{20} \\ F^{02} \end{bmatrix}^\dagger \begin{bmatrix} X & Y^* \\ Y & X^* \end{bmatrix} \times \times \begin{bmatrix} T_n\left(+\frac{\Omega}{\Omega_b}\right) & \mathbf{0} \\ \mathbf{0} & T_n\left(-\frac{\Omega}{\Omega_b}\right) \end{bmatrix} \times \times \begin{bmatrix} X & Y^* \\ Y & X^* \end{bmatrix}^{-1} \begin{bmatrix} F^{20} \\ -F^{02} \end{bmatrix}, \tag{39}$$

which after using Lemma 1 transforms to:

$$\mu_n := \lim_{\gamma\to 0^+}\mu_n^{(\gamma)} = \frac{1}{1+\delta_{n,0}}\begin{bmatrix} F^{20} \\ F^{02} \end{bmatrix}^\dagger T_n\left(\frac{1}{\Omega_b}\begin{bmatrix} \mathbf{I} & \mathbf{0} \\ \mathbf{0} & -\mathbf{I} \end{bmatrix}\begin{bmatrix} A & B \\ B^* & A^* \end{bmatrix}\right) \times \times \begin{bmatrix} \mathbf{I} & \mathbf{0} \\ \mathbf{0} & -\mathbf{I} \end{bmatrix}\begin{bmatrix} F^{20} \\ F^{02} \end{bmatrix}. \tag{40}$$

If we truncate the series (35) up to $2N_{\mathrm{it}}+1 \in \mathbb{N}$ coefficients, after taking the limit $\gamma \to 0^+$, one obtains the approximate expression for the response function:

$$\frac{dB(\omega)}{d\omega} \approx \frac{2/\pi}{\sqrt{\Omega_b^2-\omega^2}}\sum_{n=0}^{2N_{\mathrm{it}}}\mu_n T_n\left(\frac{\omega}{\Omega_b}\right), \quad \text{for } \omega \in \langle -\Omega_b, +\Omega_b\rangle, \tag{41}$$

where the coefficients $\mu_n \in \mathbb{R}$ are defined in Eq. (40). Notice that $\mu_n \in \mathbb{R}$ are indeed real because one can easily see that matrices:

$$T_n\left(\frac{1}{\Omega_b}\begin{bmatrix} \mathbf{I} & \mathbf{0} \\ \mathbf{0} & -\mathbf{I} \end{bmatrix}\begin{bmatrix} A & B \\ B^* & A^* \end{bmatrix}\right)\begin{bmatrix} \mathbf{I} & \mathbf{0} \\ \mathbf{0} & -\mathbf{I} \end{bmatrix} \in \mathbb{C}^{2N_p\times 2N_p}, \tag{42}$$

are Hermitian. Let us define a sequence of vectors $(|\alpha_n\rangle)_{n\in\mathbb{N}_0} \subseteq \mathbb{C}^{2N_p}$ as:

$$|\alpha_n\rangle := T_n\left(\frac{1}{\Omega_b}\begin{bmatrix} \mathbf{I} & \mathbf{0} \\ \mathbf{0} & -\mathbf{I} \end{bmatrix}\begin{bmatrix} A & B \\ B^* & A^* \end{bmatrix}\right)\begin{bmatrix} \mathbf{I} & \mathbf{0} \\ \mathbf{0} & -\mathbf{I} \end{bmatrix}\begin{bmatrix} F^{20} \\ F^{02} \end{bmatrix}. \tag{43}$$

Using $T_0(x) = 1$ and $T_1(x) = x$, the first two terms $|\alpha_0\rangle, |\alpha_1\rangle \in \mathbb{C}^{2N_p}$ are equal to:

$$|\alpha_0\rangle := \begin{bmatrix} F^{20} \\ -F^{02} \end{bmatrix} \text{ and } |\alpha_1\rangle := \frac{1}{\Omega_b} \begin{bmatrix} \mathbf{I} & \mathbf{0} \\ \mathbf{0} & -\mathbf{I} \end{bmatrix} \begin{bmatrix} A & B \\ B^* & A^* \end{bmatrix} \begin{bmatrix} F^{20} \\ -F^{02} \end{bmatrix}, \tag{44}$$

while the Chebyshev recursion: $T_n(x) = 2xT_{n-1}(x) - T_{n-2}(x)$, for $n \geq 2$, can be used to find other terms $|\alpha_n\rangle$ for $n \geq 2$, recursively:

$$|\alpha_n\rangle = \frac{2}{\Omega_b} \begin{bmatrix} \mathbf{I} & \mathbf{0} \\ \mathbf{0} & -\mathbf{I} \end{bmatrix} \begin{bmatrix} A & B \\ B^* & A^* \end{bmatrix} |\alpha_{n-1}\rangle - |\alpha_{n-2}\rangle. \tag{45}$$

Since there holds:

$$\mu_n = \frac{1}{1+\delta_{n,0}} \begin{bmatrix} F^{20} \\ F^{02} \end{bmatrix}^\dagger |\alpha_n\rangle, \quad \text{for} \quad n \in \mathbb{N}_0, \tag{46}$$

we can initialize the coefficients μ_0, μ_1 and use recursion (45) to find the higher coefficients μ_n, $n \geq 2$, i.e. as we calculate the nth vector $|\alpha_n\rangle$, we can calculate the nth coefficient μ_n. However, we can do better utilizing two identities:

$$T_{2n}(x) = 2T_n(x)T_n(x) - 1 \quad \text{and} \quad T_{2n-1}(x) = 2T_{n-1}(x)T_n(x) - x. \tag{47}$$

Then, one can easily show using Hermitian property of matrices (42) that there holds:

$$\mu_{2n-1} = 2\langle\alpha_{n-1}| \begin{bmatrix} \mathbf{I} & \mathbf{0} \\ \mathbf{0} & -\mathbf{I} \end{bmatrix} |\alpha_n\rangle - \mu_1, \quad n \in \mathbb{N}, \tag{48}$$

$$\mu_{2n} = 2\langle\alpha_n| \begin{bmatrix} \mathbf{I} & \mathbf{0} \\ \mathbf{0} & -\mathbf{I} \end{bmatrix} |\alpha_n\rangle - 2\mu_0, \quad n \in \mathbb{N}. \tag{49}$$

Thus, if we initialize $|\alpha_0\rangle, |\alpha_1\rangle \in \mathbb{C}^{2N_p}$ and $\mu_0, \mu_1 \in \mathbb{R}$, during the recursion (45) for each new $|\alpha_n\rangle$ we can obtain two coefficients μ_{2n-1} and μ_{2n}. Notice that for calculation of $|\alpha_0\rangle, |\alpha_1\rangle, \ldots, |\alpha_{N_{\text{it}}}\rangle$, we need to evaluate the mapping:

$$\begin{bmatrix} x \\ y \end{bmatrix} \mapsto \begin{bmatrix} A & B \\ B^* & A^* \end{bmatrix} \begin{bmatrix} x \\ y \end{bmatrix}, \tag{50}$$

exactly N_{it} times, which will yield the coefficients $\mu_0, \mu_1, \ldots, \mu_{2N_{\text{it}}}$ required in the expansion (41).

3.2. Kernel polynomial method

It is well known and can be seen from Eq. (38) that the response function $\frac{dB(\omega)}{d\omega}$ can be written as a sum of weighted delta functions centered at eigenfrequencies $\pm\Omega_i$. Experience shows that a simple truncation of Chebyshev series (41) leads to poor precision and oscillatory behavior, also known as Gibbs oscillations, near points where the expanded function is singular or discontinuous which in this case is near QRPA poles $\pm\Omega_i$. This problem has been studied in details [20] and a common procedure to damp Gibbs oscillations relies on the modification of the coefficients in the Chebyshev expansion:

$$f(x) \approx \frac{2/\pi}{\sqrt{1-x^2}} \sum_{n=0}^{N-1} \mu_n T_n(x), \quad x \in \langle -1, +1 \rangle, \tag{51}$$

with a simple transformation of expansion coefficients: $\mu_n \to \mu_n g_n^{(N)}$, for appropriate coefficients: $g_0^{(N)}, g_1^{(N)}, \ldots, g_{N-1}^{(N)}$, called the kernel coefficients. One can represent this transformation as a convolution of $f(x)$ with an appropriate kernel $K_N(x, y)$. Details can be found in Ref. [20] and here we only introduce three kernels which are most relevant for our work.

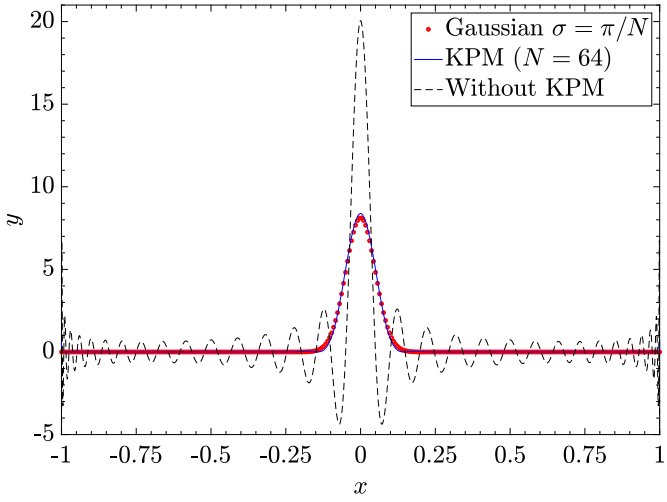

Fig. 1. (Color online) Gaussian function of width $\sigma = \pi/N$, for $N = 64$ (red circles) compared to Jackson kernel-modified Chebyshev approximation of delta function of order $N = 64$ (blue solid curve). For reference, kernel-unmodified Chebyshev approximation of delta function of order $N = 64$ is also shown (black dashed curve).

First we would like to present the Jackson kernel, designed to minimize the kernels root mean square (RMS) width. The Jackson kernel is defined as:

$$g_n^{(N)}(\text{Jackson}) := \frac{(N-n+1)\cos\left(\frac{\pi n}{N+1}\right) + \sin\left(\frac{\pi n}{N+1}\right)\cot\left(\frac{\pi}{N+1}\right)}{N+1}. \tag{52}$$

One can show that if one expands the delta function $\delta(x)$ in Chebyshev series (51), i.e. calculates the coefficients μ_n corresponding to $f(x) = \delta(x)$, followed by modifying the coefficients μ_n with Jackson kernel: $\mu_n \to \mu_n g_n^{(N)}(\text{Jackson})$, then the obtained kernel-modified Chebyshev approximation (RHS of Eq. (51)) visually resembles to a Gaussian $\frac{1}{\sqrt{2\pi}\sigma} e^{-\frac{x^2}{2\sigma^2}}$ of width $\sigma = \frac{\pi}{N}$. In Fig. 1, we plot a Gaussan of width $\sigma = \frac{\pi}{N}$, for $N = 64$, together with Jackson kernel-modified Chebyshev approximation of delta function of order $N = 64$. We also plot the kernel-unmodified Chebyshev approximation of delta function as a reference. We can see that KPM reduces the Gibbs oscillations, and the Jackson kernel-modified approximation resembles to a Gaussian of an appropriate width.

Second kernel that we present is the Lorentz kernel defined as:

$$g_n^{(N)}(\text{Lorentz}) := \frac{\sinh(\lambda(1-n/N))}{\sinh(\lambda)}, \tag{53}$$

where the value of the free parameter $\lambda > 0$ should be chosen to ensure a satisfactory compromise between good resolution (small values of the parameter λ) and sufficient damping (large values of the parameter λ). Depending on the application, the value of the λ parameter is usually chosen between values 1 and 5. In this case, if one expands the delta function as in Eq. (51), i.e. calculates the coefficients μ_n corresponding to $f(x) = \delta(x)$, followed by modifying the coefficients μ_n with Lorentz kernel: $\mu_n \to \mu_n g_n^{(N)}(\text{Lorentz})$, then the obtained kernel-modified Chebyshev approximation visually resembles to a Lorentzian $\frac{\gamma/\pi}{x^2+\gamma^2}$ with smearing parameter $\gamma = \frac{\lambda}{N}$. For example, if one selects $\lambda = 5$, the two functions: the Lorentzian having width $\gamma = \frac{\lambda}{N}$ and a Chebyshev expanded delta function with kernel-modified expansion coefficients, are virtually identical. In Fig. 2 we fix $N = 64$, and show Lorentzians of width $\gamma = \frac{\lambda}{N}$ together with Lorentz kernel-modified Chebyshev approximations of delta function of order N, as parameter λ is swept through the values $\lambda = 1, 2, 3, 4, 5$. We notice that larger

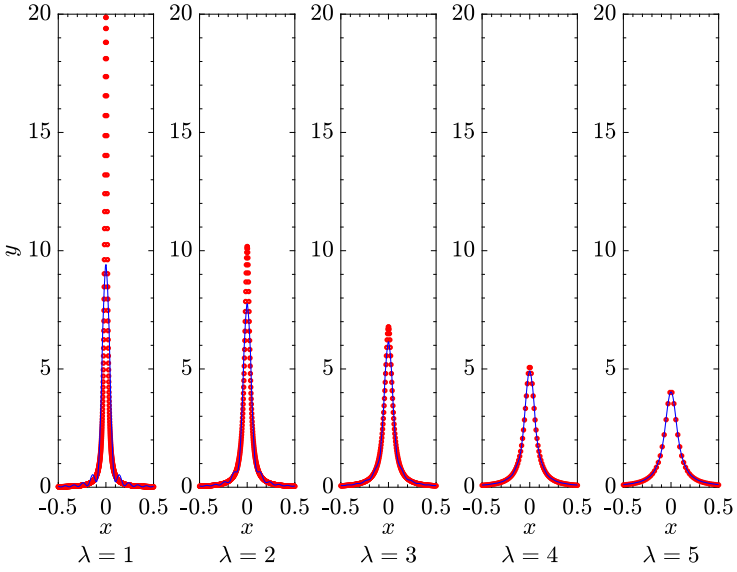

Fig. 2. (Color online) Lorentzians of width $\gamma = \frac{\lambda}{N}$ (red circles) together with Lorentz kernel-modified Chebyshev approximations of delta function of order N (blue solid curves), for a fixed value of $N = 64$ when the parameter λ is swept from values $\lambda = 1$ to $\lambda = 5$.

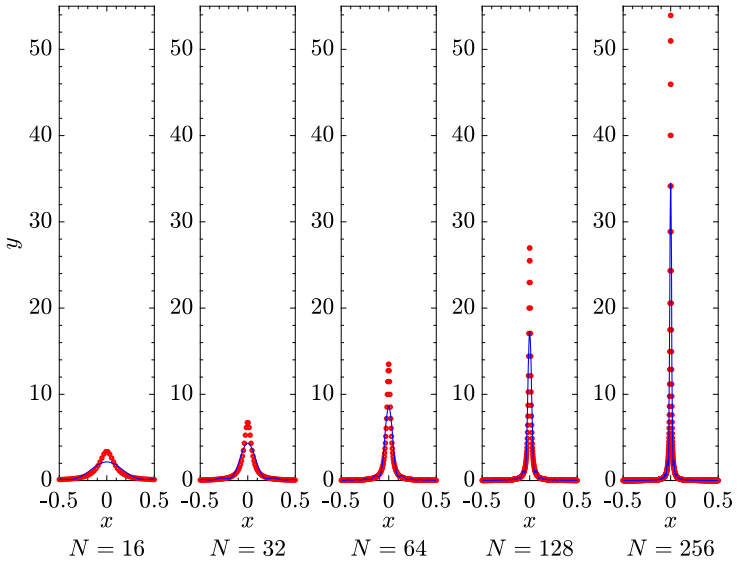

Fig. 3. (Color online) Lorentzians of width $\gamma = \frac{\lambda}{N}$ (red circles) together with Lorentz kernel-modified Chebyshev approximations of delta function of order N (blue solid curves), for a fixed value of kernel parameter $\lambda = 1.5$ when the order N is swept through the values $N = 16, 32, 64, 128, 256$.

value of λ gives better damping of the Gibbs oscillations and gives better resemblance to an appropriate Lorentzian, however, for a fixed Chebyshev approximation order N, smaller values of λ yield higher peaks and better resolution in terms of width. Thus, the value $\lambda = 1.5$ seems like a good compromise between the two. In Fig. 3, we fix $\lambda = 1.5$ parameter, and show Lorentzians of width $\gamma = \frac{\lambda}{N}$ together with Lorentz kernel-modified Chebyshev approximations of delta function of order N, as the order parameter N is swept through the values $N = 16, 32, 64, 128, 256$. Thus, for values of λ parameter below $\lambda \lessapprox 4$ the resemblance with Lorentzian is less pronounced, however the relation $\gamma = \frac{\lambda}{N}$ still approximatelly holds, but has to be taken only indicatively. Important remark to notice is that once the Chebyshev expansion coefficients μ_n are obtained (as explained in the previous subsection) one can easily choose and experiment with various kernel coefficients since they are selected *a posteriori*.

Notice that trivial transformation: $\mu_n \to 1 \cdot \mu_n$, can also be viewed as an action of constant kernel:

$$g_n^{(N)}(\text{Dirichlet}) := 1, \tag{54}$$

which is usually called the Dirichlet kernel.

In conclusion, the main goal is to damp Gibbs oscillations encountered when expanding a delta function in Chebyshev series (51), by simply multiplying the expansion coefficients μ_n with the kernel coefficient $g_n^{(N)}$, where the choice of the coefficients $g_n^{(N)}$ depends on the particular application. For example, if we want a rapidly decreasing expansion, a good choice is to use the Jackson kernel. On the other hand, if the expanded function displays the Breit-Wigner shape, such as the response function $\frac{dB(\omega)}{d\omega}$, one should use the Lorentz kernel.

3.3. Evaluation of Chebyshev series

Suppose we have calculated the coefficients $\mu_0, \mu_1, \ldots, \mu_{2N_{\text{it}}}$ in Eq. (41) and multiplied them with an appropriate kernel coefficients $g_n^{(2N_{\text{it}}+1)}$. We wish to evaluate the series (41) on a frequency grid $(\omega_k)_{k=1}^{N_e} \subseteq \langle -\Omega_b, +\Omega_b \rangle$ having N_e points for e.g. plotting or

numerical integration purpose. We can use the well known Clenshaw algorithm [25], but if we do not insist on a specific frequency grid such as uniform grid, it is better to use the Chebyshev nodes:

$$\omega_k = \Omega_b \cos\left(\frac{\pi}{N_e}\left(k-\frac{1}{2}\right)\right), \quad k = 1, 2, \ldots, N_e. \tag{55}$$

Let us assume that $N_e > N_{\text{it}}$, which is in practice always true since we usually evaluate the series on a very dense grid $N_e \gg N_{\text{it}}$. In that case we can write:

$$\frac{dB(\omega)}{d\omega} = \frac{2/\pi}{\sqrt{\Omega_b^2 - \omega^2}} \sum_{n=1}^{2N_e} \mu_{n-1} T_{n-1}\left(\frac{\omega}{\Omega_b}\right), \tag{56}$$

where the higher order coefficients: $\mu_{2N_{\text{it}}+1}, \ldots, \mu_{2N_e-1}$, are set to zero. Then there holds:

$$\frac{dB(\omega_k)}{d\omega} = \frac{2/\pi}{\Omega_b \sin\left(\frac{\pi}{N_e}\left(k-\frac{1}{2}\right)\right)} \times \times \operatorname{Re}\left[\sum_{n=1}^{2N_e}\left(\mu_{n-1} e^{-\pi \mathrm{i} \frac{(n-1)}{2N_e}}\right) e^{-2\pi \mathrm{i} \frac{(n-1)(k-1)}{2N_e}}\right]. \tag{57}$$

Previous summations can be efficiently evaluated using fast Fourier transform, e.g. freely available FFTW library [26] provides a procedure which for input sequence $x_1, x_2, \ldots, x_N \in \mathbb{C}$ calculates $X_1, X_2, \ldots, X_N \in \mathbb{C}$ defined as:

$$X_k = \sum_{n=1}^{N} x_n e^{-2\pi \mathrm{i} \frac{(n-1)(k-1)}{N}}. \tag{58}$$

Therefore, after the coefficients $\mu_0, \mu_1, \ldots, \mu_{2N_{\text{it}}}$ are calculated and kernel-readjusted, one can quickly evaluate the series (41) on a dense Chebyshev frequency grid for plotting or numerical integration purpose.

3.4. Bounding frequency

In this subsection we would like to emphasize that the bounding frequency Ω_b has to fulfill the following condition: $\pm\Omega_i \in \langle -\Omega_b, +\Omega_b\rangle$, for all $i = 1, \ldots, N_p$. Otherwise, the diagonal elements $T_n\left(\frac{\Omega_i}{\Omega_b}\right)$ in Eq. (39) are simply not defined. If the sequence of functions $T_n(x)$ is calculated recursively on $\mathbb{R}$ as $T_0(x) = 1, T_1(x) = x$ and $T_n(x) = 2xT_{n-1}(x) - T_{n-2}(x)$, then the following equation holds:

$$T_n(x) = \frac{1}{2}\left(\left(x - \sqrt{x^2-1}\right)^n + \left(x + \sqrt{x^2-1}\right)^n\right), \text{ for } |x| \geq 1. \tag{59}$$

Therefore, if the bounding frequency Ω_b does not satisfy $\pm\Omega_i \in \langle -\Omega_b, +\Omega_b\rangle$ (i.e., if $\Omega_i/\Omega_b \geq 1$), we expect that the recursive procedure (45) which generates the sequence of vectors $|\alpha_n\rangle \in \mathbb{C}^{2N_p}$ will quickly diverge. In practice, we can often provide a heuristic physical estimate of the upper bound for $\max(\Omega_i)_{i=1}^{N_p}$, and thus guess the value of Ω_b. During the recursive procedure (45), we can notice immediately if the bounding frequency is underestimated due to the divergent behavior of the μ_n coefficients. On the other hand, a more pedantic approach is to calculate the maximum eigenfrequency $\Omega_{\max} = \max(\Omega_i)_{i=1}^{N_p}$ as an extremal eigenvalue:

$$\begin{bmatrix} \mathbf{I} & \mathbf{0} \\ \mathbf{0} & -\mathbf{I} \end{bmatrix} \begin{bmatrix} A & B \\ B^* & A^* \end{bmatrix} \begin{bmatrix} X^{\max} \\ Y^{\max} \end{bmatrix} = \Omega_{\max} \begin{bmatrix} X^{\max} \\ Y^{\max} \end{bmatrix}, \quad X^{\max}, Y^{\max} \in \mathbb{C}^{N_p}. \tag{60}$$

Previous equation can be solved efficiently by employing one of the many existing iterative Krylov-space methods or power methods. The bounding frequency is then defined as $\Omega_b = \Omega_{\max} + \varepsilon$ for some small value of ε, e.g. $\varepsilon = 0.01\Omega_{\max}$. We recommend a heuristic approach for estimating Ω_b if the solver is supervised manually, although even then one can easily detect divergent behavior automatically and readjust Ω_b accordingly. For a large-scale calculations it is better to use the latter pedantic approach.

3.5. Method summary

The steps of the proposed method are summarized in Algorithm 1. We emphasize that the method is not memory intensive, since we do not need to store vectors $(|\alpha_n\rangle)_{n=0}^{N_{\text{it}}}$ in the computer memory. Keeping track of only three vectors $|\alpha_{\text{new}}\rangle, |\alpha_{\text{old}}\rangle, |\alpha_{\text{tmp}}\rangle \in \mathbb{C}^{N_p}$ will suffice to go through the recursion (45). Also, when we reach $n = N_{\text{it}}$, the algorithm stops and yields coefficients $(\mu_n)_{n=0}^{2N_{\text{it}}}$, but if the last two vectors $|\alpha_{N_{it}-2}\rangle, |\alpha_{N_{it}-1}\rangle$ are stored on drive, we can later continue calculating higher coefficients μ_n for $n > 2N_{\text{it}}$.

Algorithm 1: QRPA Chebyshev kernel polynomial method.

Input:

- QRPA matrix-vector mapping: $\begin{bmatrix} x \\ y \end{bmatrix} \in \mathbb{C}^{2N_p} \mapsto \begin{bmatrix} A & B \\ B^* & A^* \end{bmatrix}\begin{bmatrix} x \\ y \end{bmatrix} \in \mathbb{C}^{2N_p}$, with Hermitian positive-definite QRPA matrix.
- Vectors $F^{20}, F^{02} \in \mathbb{C}^{N_p}$.
- Bounding frequency $\Omega_b > 0$ satisfying $(\pm\Omega_i)_{i=1}^{N_p} \subset \langle -\Omega_b, +\Omega_b\rangle$.
- Number of iterations N_{it}, i.e. the number of matrix-vector products and number of Chebyshev nodes $N_e > N_{\text{it}}$ for evaluation of $\frac{dB(\omega)}{d\omega}$.
- Kernel coefficients $g_n^{(2N_{\text{it}}+1)}$, $n = 0, 1, \ldots, 2N_{\text{it}}$.
- Initialize $|\alpha_{\text{old}}\rangle \leftarrow |\alpha_0\rangle$, $|\alpha_{\text{new}}\rangle \leftarrow |\alpha_1\rangle$ according to Eq. (44):

$$|\alpha_{\text{old}}\rangle \leftarrow \begin{bmatrix} F^{20} \\ -F^{02} \end{bmatrix} \text{ and } |\alpha_{\text{new}}\rangle \leftarrow \frac{1}{\Omega_b}\begin{bmatrix} \mathbf{I} & \mathbf{0} \\ \mathbf{0} & -\mathbf{I} \end{bmatrix}\begin{bmatrix} A & B \\ B^* & A^* \end{bmatrix}\begin{bmatrix} F^{20} \\ -F^{02} \end{bmatrix}. \tag{61}$$

- Initialize μ_0 and μ_1 according to Eq. (46):

$$\mu_0 \leftarrow \frac{1}{2}\begin{bmatrix} F^{20} \\ F^{02} \end{bmatrix}^{\dagger} |\alpha_{\text{old}}\rangle \text{ and } \mu_1 \leftarrow \begin{bmatrix} F^{20} \\ F^{02} \end{bmatrix}^{\dagger} |\alpha_{\text{new}}\rangle. \tag{62}$$

for $n = 1, 2, \ldots, N_{it}$ **do**

// Now there holds: $|\alpha_{new}\rangle = |\alpha_n\rangle$ *and* $|\alpha_{old}\rangle = |\alpha_{n-1}\rangle$.

- Calculate μ_{2n-1} and μ_{2n} according to Eq. (48) and (49):
  - $\mu_{2n-1} \leftarrow 2\langle\alpha_{\text{old}}|\begin{bmatrix} \mathbf{I} & \mathbf{0} \\ \mathbf{0} & -\mathbf{I} \end{bmatrix}|\alpha_{\text{new}}\rangle - \mu_1$,
  - $\mu_{2n} \leftarrow 2\langle\alpha_{\text{new}}|\begin{bmatrix} \mathbf{I} & \mathbf{0} \\ \mathbf{0} & -\mathbf{I} \end{bmatrix}|\alpha_{\text{new}}\rangle - 2\mu_0$.
- If μ_{2n-1}, μ_{2n} start to diverge, Ω_b is too small, restart with new Ω_b!
- If $n < N_{\text{it}}$, update vectors $|\alpha_{\text{new}}\rangle, |\alpha_{\text{old}}\rangle$ according to Eq. (45):
  - $|\alpha_{\text{tmp}}\rangle \leftarrow |\alpha_{\text{new}}\rangle$,
  - $|\alpha_{\text{new}}\rangle \leftarrow \frac{2}{\Omega_b}\begin{bmatrix} \mathbf{I} & \mathbf{0} \\ \mathbf{0} & -\mathbf{I} \end{bmatrix}\begin{bmatrix} A & B \\ B^* & A^* \end{bmatrix}|\alpha_{\text{new}}\rangle - |\alpha_{\text{old}}\rangle$,
  - $|\alpha_{\text{old}}\rangle \leftarrow |\alpha_{\text{tmp}}\rangle$.

end

- Apply kernel transformation $\mu_n \leftarrow g_n^{(2N_{\text{it}}+1)}\mu_n$, for $n = 0, 1, \ldots, 2N_{\text{it}}$.
- Evaluate $\frac{dB(\omega_k)}{d\omega}$ on Chebyshev nodes $(\omega_k)_{k=1}^{N_e}$ using Eq. (57) via FFT.

Output: Truncated Chebyshev expansion of the response function $\frac{dB(\omega)}{d\omega}$ as in Eq. (41) evaluated on Chebyshev frequency nodes (55).

4. Numerical results

To validate our implementation of the KPM for calculating the QRPA response function, as described in Algorithm 1, we have performed several test calculations. All tests are available at the public GitHub repository [27] in a form of MATLAB scripts, tested on the MATLAB releases R2018a and R2021a. We have also verified that scripts are running with GNU Octave 5.2.0 as a publicly available alternative which is mostly compatible with MATLAB. We notice that for some calculations Octave is considerably slower in comparison to MATLAB. To reduce the computation time, we have

included the recommended values of numerical parameters to be used with Octave in the scripts that would otherwise be time consuming.

4.1. Test 1: synthetic model

For our first test case we use synthetically generated QRPA matrices A, B and vectors F^{20}, F^{02} by employing the procedure described in Appendix B. The matrix dimension and the bounding frequency are set to $N_p = 1000$ and $\Omega_b = 250$ MeV, respectively. 500 random eigenfrequencies Ω_i are generated uniformly in range from 0 MeV to 200 MeV and combined with another 500 random eigenfrequencies Ω_i generated uniformly in range from 0 MeV to 50 MeV. The resulting QRPA spectrum will obviously be more dense in the low energy region. Next, we generate random sequence of values $\theta_1, \ldots, \theta_{N_p} \geq 0$ and two unitary matrices $C, D \in \mathbb{C}^{N_p \times N_p}$ as Q factors in the QR decomposition of two random $N_p \times N_p$ complex matrices. The X and Y matrices are constructed as:

$$X = D\,\mathrm{diag}[\cosh\theta_i]_{i=1}^{N_p} C \quad \text{and} \quad Y = D^*\,\mathrm{diag}[\sinh\theta_i]_{i=1}^{N_p} C, \tag{63}$$

and used to generate the A and B matrices:

$$A = +\left[X\Omega X^\dagger + \left(Y\Omega Y^\dagger\right)^*\right] \quad \text{and} \quad B = -\left[X\Omega Y^\dagger + \left(X\Omega Y^\dagger\right)^T\right], \tag{64}$$

as explained in Remark 1.

Notice that from Eq. (32) the response function $\frac{dB(\omega)}{d\omega}$ can be written as:

$$\frac{dB(\omega)}{d\omega} = \sum_{i=1}^{N_p} |\langle i|\hat{F}|0\rangle|^2 \delta(\omega - \Omega_i) - \sum_{i=1}^{N_p} |\langle 0|\hat{F}|i\rangle|^2 \delta(\omega + \Omega_i), \tag{65}$$

where vectors $(\langle i|\hat{F}|0\rangle)_{i=1}^{N_p} \in \mathbb{C}^{N_p}$ and $(\langle i|\hat{F}|0\rangle)_{i=1}^{N_p} \in \mathbb{C}^{N_p}$ are defined as:

$$\begin{bmatrix} (\langle i|\hat{F}|0\rangle)_{i=1}^{N_p} \\ (\langle 0|\hat{F}|i\rangle)_{i=1}^{N_p} \end{bmatrix} = \begin{bmatrix} X & Y^* \\ Y & X^* \end{bmatrix}^\dagger \begin{bmatrix} F^{20} \\ F^{02} \end{bmatrix}. \tag{66}$$

The real and imaginary parts of the matrix elements $\langle i|\hat{F}|0\rangle$ are generated from the standard normal distribution and since we assume that the operator $\hat{F}$ is Hermitian. We set: $\langle 0|\hat{F}|i\rangle = \langle i|\hat{F}|0\rangle^*$.

Finally, we construct vectors $F^{20}, F^{02} \in \mathbb{C}^{N_p}$ so that Eq. (66) is satisfied:

$$\begin{bmatrix} F^{20} \\ F^{02} \end{bmatrix} = \begin{bmatrix} \mathbf{I} & \mathbf{0} \\ \mathbf{0} & -\mathbf{I} \end{bmatrix} \begin{bmatrix} X & Y^* \\ Y & X^* \end{bmatrix} \begin{bmatrix} \mathbf{I} & \mathbf{0} \\ \mathbf{0} & -\mathbf{I} \end{bmatrix} \begin{bmatrix} (\langle i|\hat{F}|0\rangle)_{i=1}^{N_p} \\ (\langle 0|\hat{F}|i\rangle)_{i=1}^{N_p} \end{bmatrix}. \tag{67}$$

In Fig. 4 we display the response function Eq. (65) calculated on the interval $\langle -\Omega_b, +\Omega_b\rangle$ for one such generated example. Next, we will try to reproduce this response function by employing the KPM. We select the allowed number of the QRPA matrix-vector multiplications N_{it} and perform steps of Algorithm 1, using the Lorentz kernel with parameter $\lambda = 1.5$. The results are shown in Fig. 5 on the low-energy interval from 0 MeV to 50 MeV, where we increase N_{it} from 200 up to 6400 iterations, each time doubling the value of N_{it}. Since the Lorentz kernel approximates delta functions in eq. (65) with Lorentzian distributions of width:

$$\gamma_{\mathrm{KPM}} = \Omega_b \frac{\lambda}{2N_{\mathrm{it}} + 1}, \tag{68}$$

we expect that doubling the number of iterations N_{it} in Algorithm 1 will yield the sum of two times narrower Lorentzians. For comparison, we also plotted in Fig. 5 a true response function folded with a Lorentzian of width $\gamma = 0.05$ MeV:

$$\left.\frac{dB(\omega)}{d\omega}\right|_\gamma = \sum_{i=1}^{N_p} |\langle i|\hat{F}|0\rangle|^2 \frac{\gamma/\pi}{(\omega - \Omega_i)^2 + \gamma^2} - \sum_{i=1}^{N_p} |\langle 0|\hat{F}|i\rangle|^2 \frac{\gamma/\pi}{(\omega + \Omega_i)^2 + \gamma^2}. \tag{69}$$

In Fig. 6 we show a zoom of the response function for frequency in range from 0 MeV to 10 MeV and $N_{\mathrm{it}} = 6400$. We notice that some artefacts of the Gibbs oscillations are still present and although they could be further damped by increasing the Lorentz kernel parameter λ, this would require more iterations N_{it} in Algorithm 1 according to Eq. (68) in order to obtain the same γ_{KPM}. We have found that $\lambda \approx 1.5$ provides a good compromise between speed and accuracy of the KPM calculation. From Eq. (68) it follows that one should select the smallest possible bounding frequency Ω_b (but still larger than the largest eigenfrequency $\Omega_{\max}$) in order to minimize the necessary number of iterations N_{it} for the targeted smearing width γ_{KPM}, assuming fixed λ parameter.

We can conclude that the proposed implementation of the KPM to calculate the QRPA response function successfully reproduces the results obtained by direct diagonalization of synthetically generated QRPA matrix. We have also verified that the same results are obtained if linear response equations (25) are solved for a range of frequencies ω with fixed $\gamma = 0.05$ MeV.

4.2. Test 2: matrix RPA solver

In this test, we would like to validate the KPM implementation for calculating the RPA response function when applied to a realistic RPA solver. For this purpose we have selected publicly available RPA solver `skyrme_rpa` [28]. This solver is implemented for closed shell spherical nuclei with Skyrme-type interactions. The Hartree-Fock equations are solved on a radial mesh using the box boundary condition and the RPA matrix is explicitly constructed and diagonalized for a given value of total angular momentum and parity J^π. The output of the `skyrme_rpa` solver contains calculated eigenfrequencies and transition strengths for isoscalar and isovector multipole operators $\hat{F}^{IS/IV}_{J^\pi}$. Also, the isoscalar and isovector response functions (69) folded with Lorentzian functions of selected width γ are provided.

We have modified the `skyrme_rpa` code and extracted the RPA matrices A and B and vectors F^{20}, F^{02} for the ^{120}Sn isotope and $J^\pi = 5^-$ isovector operator. Calculation was performed by employing the SLy5 Skyrme interaction [29] in a 20 fm radius box with 0.1 fm radial step and 100 MeV cutoff energy.[1] The resulting $2N_p \times 2N_p$ RPA matrix is of order $N_p = 1310$. Based on the value of the cutoff energy E_c, we do not expect that the particle-hole energies will be larger than ≈ 250 MeV, therefore we set the value of the bounding frequency to $\Omega_b = 250$ MeV. Indeed, we have verified that the largest calculated RPA eigenfrequency is $\Omega_{\max} = 156$ MeV. In order to damp Gibbs oscillations, Lorentzian kernel with parameter $\lambda = 1.5$ was used. Fig. 7 displays the response function obtained by the original `skyrme_rpa` code folded with the Lorentzian function of width $\gamma = 0.05$ MeV in comparison to the results obtained using the KPM with $N_{\mathrm{it}} = 6400$ iterations. It is worth noting that the necessary number of iterations N_{it} could

[1] Cutoff energy E_c denotes maximum energy of the unoccupied single-particle states included in the RPA model space. The maximum particle–hole energy is thus $E_c - \epsilon_h$, where ϵ_h is the deepest hole energy. For the chosen value $E_c = 100$ MeV, rough estimate of the maximum particle-hole energy is ≈ 150 MeV.

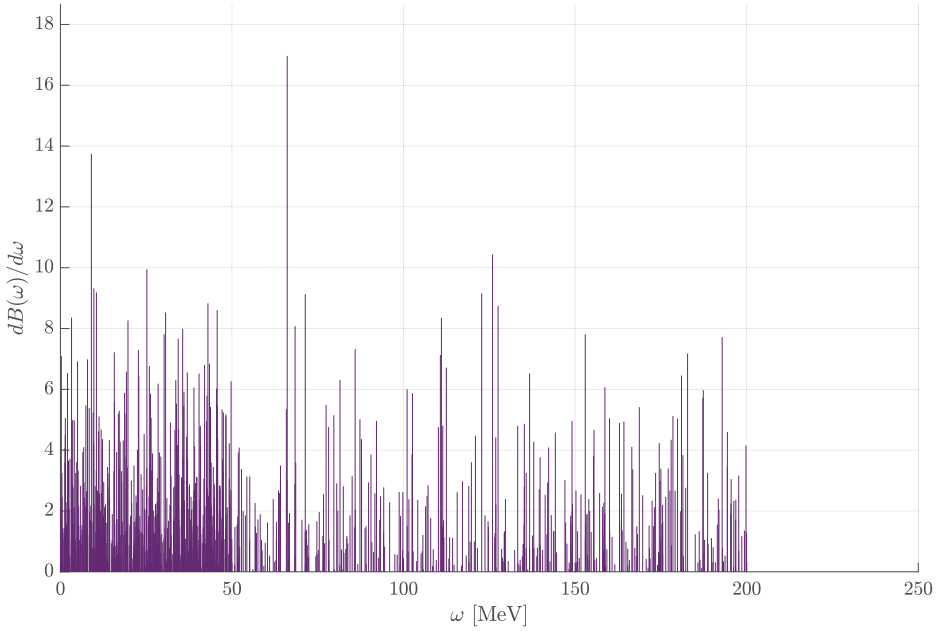

Fig. 4. (Color online) Synthetically generated response function $\frac{dB(\omega)}{d\omega}$ calculated by using Eq. (65). The positions of the vertical lines are given by the eigenfrequencies Ω_i, while the heights are equal to $|\langle i|\hat{F}|0\rangle|^2$.

be reduced by choosing the bounding frequency Ω_b closer to the largest RPA eigenfrequency $\Omega_{\max}$.

In Fig. 8 we display a zoom of the response functions shown in Fig. 7 for frequency in range from 20 MeV to 30 MeV. The two response functions are virtually identical although there are still some Gibbs oscillation effects visible in the response function calculated by the KPM.

4.3. Test 3: quasiparticle finite amplitude method solver

Next, we would like to validate the KPM implementation for calculating the QRPA response function when applied in conjunction with a realistic QFAM solver. Similar to the previous test, we have selected publicly available finite amplitude method solver `DIRQFAM` [30]. The `DIRQFAM` code calculates the QRPA multipole response of even–even open-shell nuclei with axially deformed ground state using the finite amplitude method, based on the relativistic self-consistent mean-field models. The QFAM amplitudes are expanded in the basis of the eigenfunctions of the axially symmetric harmonic oscillator with simplex-y symmetry imposed. The `DIRQFAM` code iteratively solves the QFAM equations for a given frequency ω_γ:

$$(E_\mu + E_\nu - \omega_\gamma)X_{\mu\nu}(\omega_\gamma) + \delta H^{20}_{\mu\nu}(\omega_\gamma) = -F^{20}_{\mu\nu}, \tag{70}$$

$$(E_\mu + E_\nu + \omega_\gamma)Y_{\mu\nu}(\omega_\gamma) + \delta H^{02}_{\mu\nu}(\omega_\gamma) = -F^{02}_{\mu\nu}. \tag{71}$$

It should be emphasized that the QFAM calculations can be performed very efficiently by using the self-consistent symmetries of the ground state,[2] together with the structure of the excitation operator $\hat{F}$. For initial guess of the QFAM amplitudes we usually choose:

$$X_{\mu\nu}(\omega_\gamma) = Y_{\mu\nu}(\omega_\gamma) = 0, \tag{72}$$

and during the iterations QFAM equations preserve the symmetry of the excitation operator. For example, if the excitation operator proportional to the spherical harmonic $Y_{JK}(\theta,\phi)$ is used, all matrices involved in the calculations turn out to have block structure and the induced densities and currents have simple $\cos(K\phi)$ or $\sin(K\phi)$ angular dependence. By utilizing these properties, the computational cost of the QFAM calculations is reduced drastically.

At the core of any QFAM solver is the implementation of the linear mapping:

$$\begin{bmatrix} X_{\mu\nu} \\ Y_{\mu\nu} \end{bmatrix} \mapsto \begin{bmatrix} \delta H^{20}_{\mu\nu} \\ \delta H^{02}_{\mu\nu} \end{bmatrix} = \begin{bmatrix} -(E_\mu + E_\nu)X_{\mu\nu} + \sum_{\mu'<\nu'} A_{\mu\nu,\mu'\nu'}X_{\mu'\nu'} + B_{\mu\nu,\mu'\nu'}Y_{\mu'\nu'} \\ -(E_\mu + E_\nu)Y_{\mu\nu} + \sum_{\mu'<\nu'} B^*_{\mu\nu,\mu'\nu'}X_{\mu'\nu'} + A^*_{\mu\nu,\mu'\nu'}Y_{\mu'\nu'} \end{bmatrix}, \tag{73}$$

which together with the QFAM equations (70) and (71) is used to solve these equations iteratively. However, the `DIRQFAM` solver does not implement the full mapping (73) for arbitrary amplitudes $X_{\mu\nu}, Y_{\mu\nu}$, but rather only for those belonging to the linear subspace defined by the self-consistent symmetries of the ground state and structure of the excitation operator (see [30] for details on the `DIRQFAM` code). Therefore, it seems that we might encounter problems implementing the KPM since the `DIRQFAM` code actually has no access to the full mapping:

$$\begin{bmatrix} x \\ y \end{bmatrix} \in \mathbb{C}^{2N_p} \mapsto \begin{bmatrix} A & B \\ B^* & A^* \end{bmatrix} \begin{bmatrix} x \\ y \end{bmatrix} \in \mathbb{C}^{2N_p}, \tag{74}$$

required by the Algorithm 1. However, the algorithm initializes vectors $|\alpha_{\text{old}}\rangle$, $|\alpha_{\text{new}}\rangle$ as in Eq. (61) which are consistent with the selection rules of the excitation operator and all selection rules are preserved throughout the recursion in Algorithm 1. This means that the KPM for calculating the QRPA response function does not require the full mapping (74), but only restricted mapping on vectors consistent with the selection rules of the particular excitation operator. This point is very important in practical calculations because virtually every QFAM solver assumes some form of symmetry in order to reduce the computational complexity.

[2] In the `DIRQFAM` code one assumes the axial symmetry, parity and time-reversal invariance in the ground state.

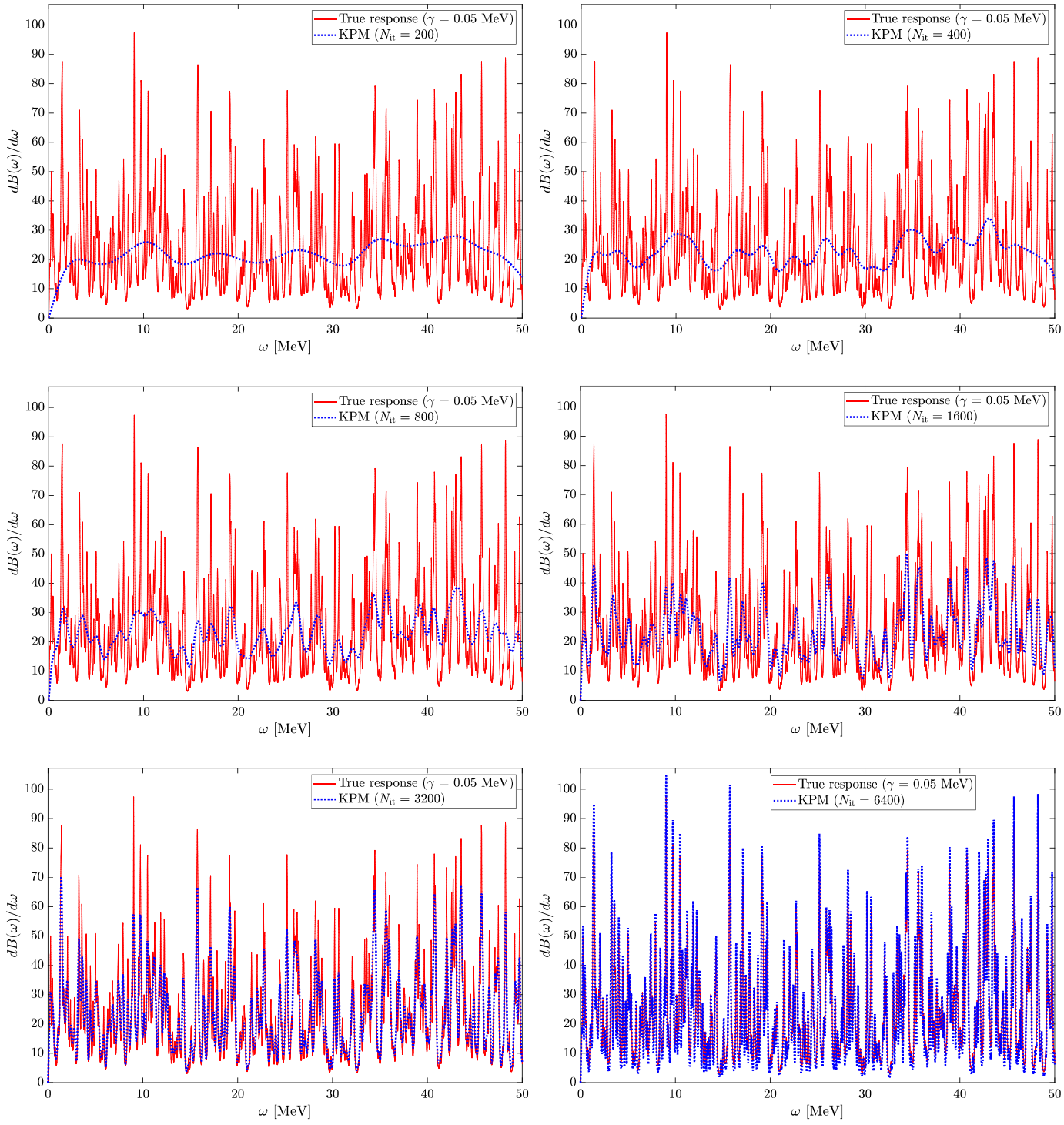

Fig. 5. (Color online) True response function (solid red curve) folded with Lorentzian of width $\gamma = 0.05$ MeV in comparison to the response function calculated by using Algorithm 1 (dot-dashed blue curve) as the number of QRPA matrix-vector multiplications $N_{\rm it}$ increases from 200 to 6400. We plot only the low-energy region from 0 MeV to 50 MeV.

For the purpose of this test, we have selected the ^{100}Zr nucleus with deformed ground state ($\beta \approx 0.485$), subjected to the isovector octupole $J = 3$, $K = 3$ excitation. In the particle-hole channel we employ the DD-PC1 [31] effective interaction, while the particle-particle channel is described by a separable finite-range force [32]. Dirac spinors are expanded in the basis of the eigenfunctions of the axially symmetric harmonic oscillator with 14 major shells for large and 15 major shells for small components. First, for comparison purpose, we have performed the QFAM calculation sweeping through frequencies from 0 MeV to 50 MeV and using the smearing $\gamma = 0.05$ MeV. Then, we employ Algorithm 1 with Lorentz kernel with parameter $\lambda = 1.5$. In order to obtain an assessment of the bounding frequency, we need a rough approximation of the QRPA eigenfrequencies $(\Omega_i)_{i=1}^{N_p}$. As a starting point, we can ignore the residual interaction $\delta H^{20}_{\mu\nu} = \delta H^{02}_{\mu\nu} = 0$ in QFAM equations (70) and (71) (often refereed to as the free response) which yields the lowest order approximation value of the largest QRPA eigenfrequency:

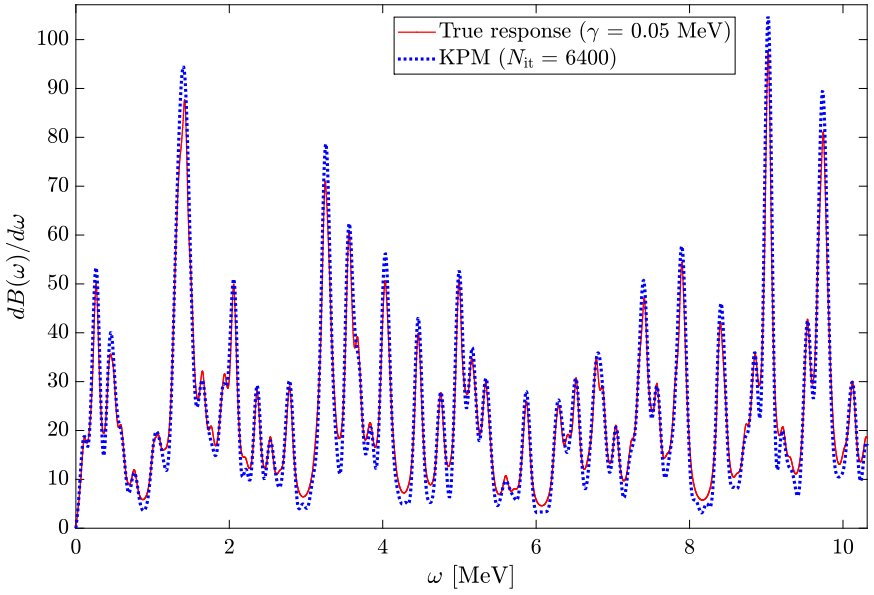

Fig. 6. (Color online) Zoom of the response function displayed in Fig. 5 for frequency in range from 0 MeV to 10 MeV. The number of iterations used is $N_{\rm it} = 6400$.

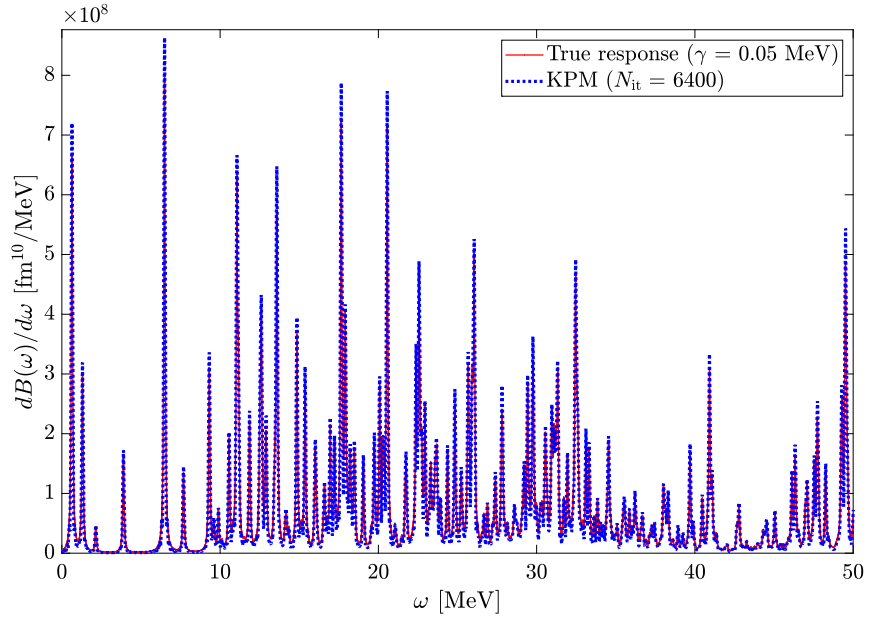

Fig. 7. (Color online) Comparison of the response functions obtained by using the original `skyrme_rpa` code (red curve) and the KPM (blue curve) for the ^{120}Sn isotope and isovector $J^\pi = 5^-$ excitation.

$$\Omega_{\rm max} \approx \max_{\mu\nu} \left| E_\mu + E_\nu \right| \leq 2 \max_\mu |E_\mu|. \tag{75}$$

Since `DIRQFAM` solver relies on the relativistic EDFs, configuration space includes, not only the Fermi sea, but also the Dirac sea of negative energy states. In addition to the configurations built from two-quasiparticle states of positive energy, the configuration space must also contain pair-configurations formed from the fully or partially occupied states of positive energy and the empty negative-energy states from the Dirac sea. The inclusion of configurations built from occupied positive-energy states and empty negative-energy states is essential for current conservation and the decoupling of spurious states [33]. Since the energies of the states in Dirac sea reach typical values of $E_\mu \approx -2000$ MeV, the value of the maximal QRPA eigenfrequency is very large and thus we have to use a comparable value of the bounding frequency Ω_b. In this particular test we use the value $\Omega_b = 4500$ MeV. Indeed, the Algorithm 1 diverges quickly if one tries to reduce the bounding frequency below 4000 MeV. This behavior suggests that the KPM is not well suited for calculations based on the relativistic EDFs, because according to the Eq. (68) we would have to perform a large number of iterations $N_{\rm it}$ in order to obtain a reasonably sharp resolution $\gamma_{\rm KPM}$ of the KPM approximation of the response function. Nevertheless, since `DIRQFAM` code is the only publicly available QFAM solver at this time, for demonstration purpose we have implemented the KPM in conjunction with this solver. In Fig. 9 we show the response function for the $J = 3$, $K = 3$ excitation built on top of the deformed ground state in the ^{100}Zr. Results obtained with the `DIRQFAM` code (solid red line) are compared with those obtained by the KPM implementation (dotted blue line). A large number of iterations $N_{\rm it} = 100000$ was used in the KPM calculation due to the effects of the Dirac sea. In Fig. 10 we show a zoom of the response function displayed in Fig. 9 for frequencies in range from 20 MeV to 40 MeV. If we estimate that one typically requires

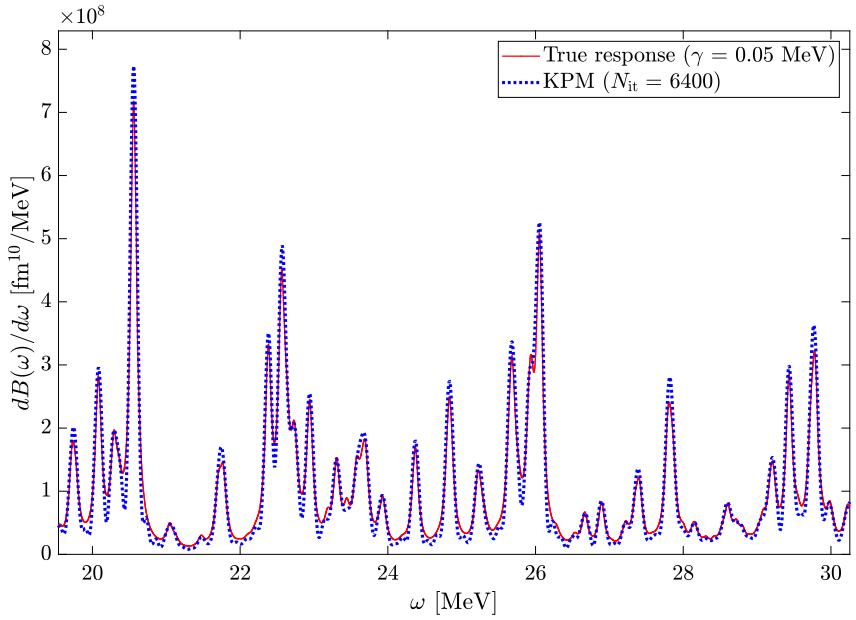

Fig. 8. (Color online) Zoom of the response function displayed in Fig. 7 for energy in range from 20 MeV to 30 MeV.

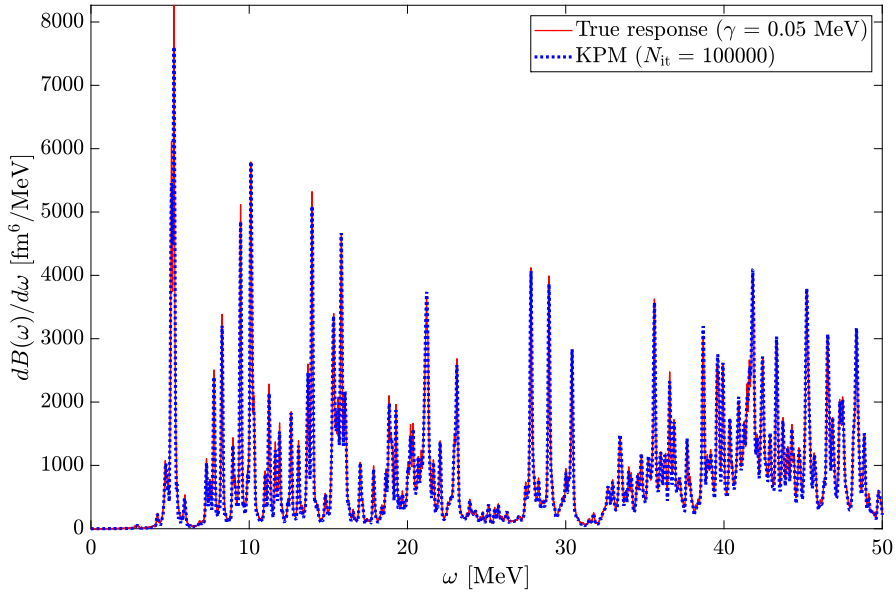

Fig. 9. (Color online) Comparison of the response functions obtained using the original DIRQFAM code and the proposed method for deformed ($\beta \approx 0.485$) isotope ^{100}Zr subjected to isovector $J = 3, K = 3$ excitation.

50 QFAM iterations to find the QFAM response at any given frequency ω_γ, in 100000 QFAM iterations we would have obtained 2000 points $\left(\omega_\gamma, \frac{dB(\omega)}{d\omega}\Big|_\gamma\right)$ which is more than enough to display a good approximation of the response function on energy interval 0-50 MeV even for a small smearing γ.

In the QRPA calculations, sometimes one encounters zero-energy modes known as the Nambu-Goldstone (NG) modes. The NG modes originate from the broken symmetries on the mean-field level of the calculation: translational symmetry, rotational symmetry and particle-number (gauge) symmetry. Since the NG modes do not represent physical excitations, they are also referred to as spurious modes. So far, we have used the XY representation of the QRPA and assumed that the QRPA matrix is positive definite, yielding $\Omega_i > 0$. The XY representation is not adequate to treat the zero-energy NG modes because they are not normalizable in this representation and, in principle, one should switch to the QP representation (for extensive discussion see Ref. [34] and references cited therein). However, due to the various numerical inaccuracies in practical calculations (e.g. single-particle states are expanded in the finite harmonic oscillator basis or in the coordinate lattice of a finite box), the frequency of the NG modes is small but still finite. Hence, such states can still be safely treated in the XY representation. To illustrate this, we analyze the $K^\pi = 1^+$ spurious mode originating from broken rotational symmetry. In Fig. 11 we display the response functions for the $J = 2$, $K = 1$ excitation operator built on top of the deformed ground state of the ^{100}Zr isotope. A zoom of Fig. 11 is shown in Fig. 12 with smaller span on the vertical axis. Indeed we observe one dominant spurious mode originating from the broken rotational symmetry and again we find an excellent agreement between the DIRQFAM and KPM response. We have also verified that the KPM method successfully

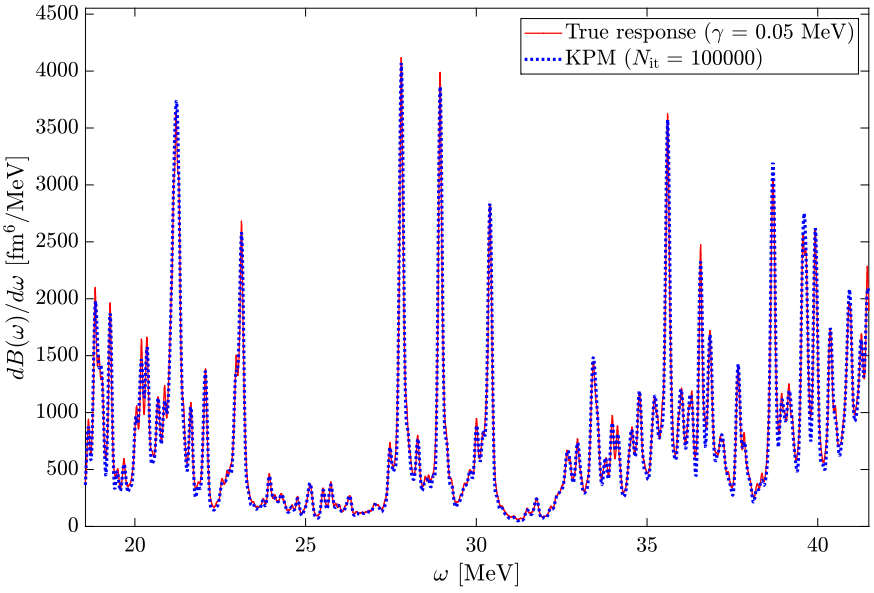

Fig. 10. (Color online) Zoom of the response function displayed in Fig. 9 for frequencies in range from 20 MeV to 40 MeV.

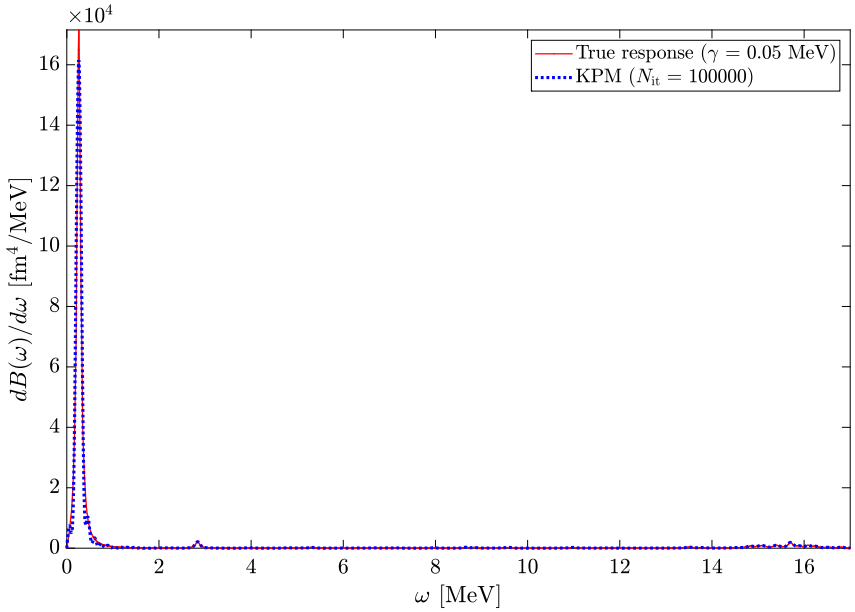

Fig. 11. (Color online) Comparison of the response functions obtained using the original DIRQFAM code and the KPM for deformed ^{100}Zr isotope subjected to the isoscalar $J = 2$, $K = 1$ excitation.

reproduces the DIRQFAM $K^\pi = 0^+$ response to the particle number operator. In this case, only the NG mode is present and the KPM is still applicable. We notice that the DIRQFAM solver separates the spurious center of mass $K^\pi = 1^-$ mode from physical modes by using a method described in Ref. [9].

Finally, we would like to emphasize that in the presence of imaginary QRPA eigenfrequency[3] the KPM calculation diverges. Essentially, the KPM deals with the Chebyshev polynomials evaluated at the eigenfrequencies: $T_n\left(\frac{\Omega_i}{\Omega_b}\right)$, as can be seen from Eq. (39). Since $T_n(ix)$ diverges as n increases for $x > 0$, one can easily see that the existence of eigenfrequency with significant imaginary part yields a fast divergence of the KPM method. On the other hand, such a fast divergence can be used as a clear indicator that one is performing calculation based on the stability matrix which is not positive definite.

In conclusion, we have demonstrated as a proof-of-concept that Algorithm 1 can be rapidly integrated into an existing QFAM solver (e.g. additional ≈ 300 lines of code in the DIRQFAM solver). However, the method is not well suited for models based on the relativistic energy density functionals because of the contributions from the states in the Dirac sea, and it diverges if the calculated ground state does not correspond to the HFB minimum.

4.4. Test 4: moments of the response function

It is well known that the sum rules represent a very important tool in studies of collective excitation, especially giant resonances

[3] E.g. if one tries to perform the spherical $J^\pi = 2^+$ QRPA calculation on a nucleus with deformed ground state. In this case the constrained spherical configuration on top of which the QRPA calculation is performed does not correspond to the HFB minimum and therefore the HFB stability matrix, i.e., the QRPA matrix, is not positive definite.

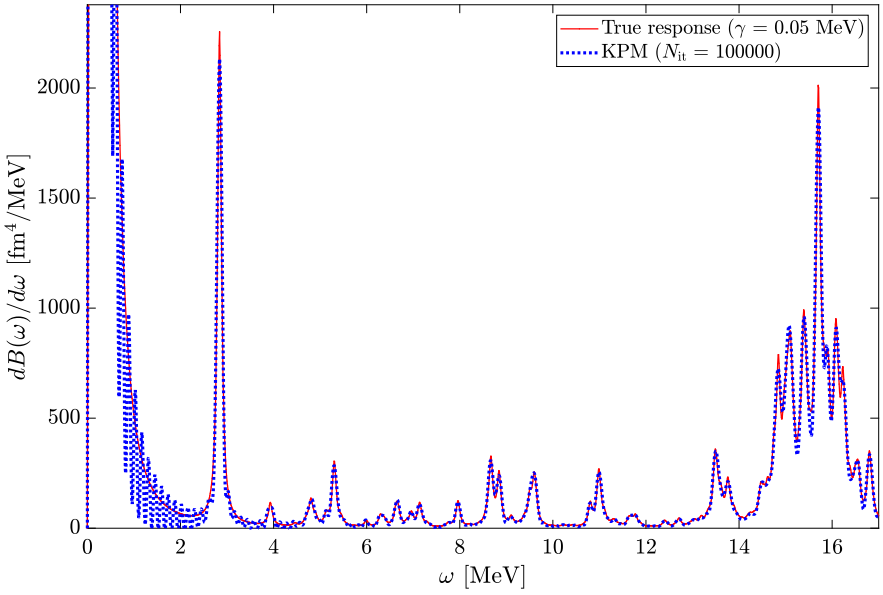

Fig. 12. (Color online) Zoom of the response function displayed in Fig. 11 with smaller span on the vertical axis.

[7]. Although sum rules provide less detailed description of the response function in comparison to the full QRPA calculation, they are still very useful for calculating the global properties of the response function. In this section we show how the Chebyshev expansion of the response function Eq. (41) can be used to calculate the moments defined as:

$$m_k = \sum_{i=1}^{N_p} \Omega_i^k |\langle i|\hat{F}|0\rangle|^2, \quad \text{for } k \in \mathbb{Z}. \tag{76}$$

From Eq. (65) one easily sees:

$$m_k = \int_0^{+\infty} \omega^k \frac{dB(\omega)}{d\omega} d\omega. \tag{77}$$

We assume that the excitation operator $\hat{F}$ is Hermitian giving $\langle 0|\hat{F}|i\rangle = \langle i|\hat{F}|0\rangle^*$ and consequently $\left(F^{02}\right)^* = F^{20}$. First we focus on the odd moments $k \in \mathbb{Z}$ since they can be efficiently calculated directly [35]. Recall the Lemma 1 and equation:

$$\begin{bmatrix} \mathbf{I} & \mathbf{0} \\ \mathbf{0} & -\mathbf{I} \end{bmatrix} \begin{bmatrix} A & B \\ B^* & A^* \end{bmatrix} = \begin{bmatrix} X & Y^* \\ Y & X^* \end{bmatrix} \begin{bmatrix} +\Omega & \mathbf{0} \\ \mathbf{0} & -\Omega \end{bmatrix} \begin{bmatrix} X & Y^* \\ Y & X^* \end{bmatrix}^{-1}. \tag{78}$$

Notice that for any $k \in \mathbb{Z}$ (even for negative) the following equation holds:

$$\left(\begin{bmatrix} \mathbf{I} & \mathbf{0} \\ \mathbf{0} & -\mathbf{I} \end{bmatrix} \begin{bmatrix} A & B \\ B^* & A^* \end{bmatrix} \right)^k = \begin{bmatrix} X & Y^* \\ Y & X^* \end{bmatrix} \begin{bmatrix} (+\Omega)^k & \mathbf{0} \\ \mathbf{0} & (-\Omega)^k \end{bmatrix} \begin{bmatrix} X & Y^* \\ Y & X^* \end{bmatrix}^{-1}. \tag{79}$$

By using Eqs. (29) and (67), one can easily show:

$$\begin{bmatrix} F^{20} \\ F^{02} \end{bmatrix}^\dagger \left(\begin{bmatrix} \mathbf{I} & \mathbf{0} \\ \mathbf{0} & -\mathbf{I} \end{bmatrix} \begin{bmatrix} A & B \\ B^* & A^* \end{bmatrix} \right)^k \begin{bmatrix} \mathbf{I} & \mathbf{0} \\ \mathbf{0} & -\mathbf{I} \end{bmatrix} \begin{bmatrix} F^{20} \\ F^{02} \end{bmatrix} = \sum_{i=1}^{N_p} (+\Omega_i)^k |\langle i|\hat{F}|0\rangle|^2 - \sum_{i=1}^{N_p} (-\Omega_i)^k |\langle 0|\hat{F}|i\rangle|^2. \tag{80}$$

Using the fact that $k \in \mathbb{Z}$ is odd integer and $\langle 0|\hat{F}|i\rangle = \langle i|\hat{F}|0\rangle^*$ we finally obtain:

$$m_k = \sum_{i=1}^{N_p} \Omega_i^k |\langle i|\hat{F}|0\rangle|^2 = \frac{1}{2} \begin{bmatrix} F^{20} \\ F^{02} \end{bmatrix}^\dagger \left(\begin{bmatrix} \mathbf{I} & \mathbf{0} \\ \mathbf{0} & -\mathbf{I} \end{bmatrix} \begin{bmatrix} A & B \\ B^* & A^* \end{bmatrix} \right)^k \begin{bmatrix} \mathbf{I} & \mathbf{0} \\ \mathbf{0} & -\mathbf{I} \end{bmatrix} \begin{bmatrix} F^{20} \\ F^{02} \end{bmatrix}. \tag{81}$$

Notice that m_k is indeed a real number. If $k > 0$, Eq. (81) can be used to evaluate m_k by applying the mapping Eq. (74) k times. On the other hand, if $k < 0$, one has to solve the linear system k times with invertible matrix:

$$\begin{bmatrix} \mathbf{I} & \mathbf{0} \\ \mathbf{0} & -\mathbf{I} \end{bmatrix} \begin{bmatrix} A & B \\ B^* & A^* \end{bmatrix}. \tag{82}$$

This is exactly what the QFAM solver does when finding the QFAM amplitudes $X_{\mu\nu}(\omega_\gamma), Y_{\mu\nu}(\omega_\gamma)$ for fixed frequency ω_γ, i.e. when solving the linear equation (25) having only access to the mapping (74). In conclusion, if $k \in \mathbb{Z}$ is odd, QFAM solver can use equation (81) to efficiently calculate the odd moments m_k directly. We have validated Eq. (81) on synthetically generated examples used in Sec. 4.1 and on realistic example used in Sec. 4.2.

Now we turn to a more difficult case, where $k \in \mathbb{Z}$ is an even integer. Also, we assume that $k \geq 0$. Since all the eigenfrequencies are located in an interval $\langle -\Omega_b, +\Omega_b \rangle$, when inserting the expansion (41) into Eq. (77), we obtain:

$$m_k = \int_0^{\Omega_b} \omega^k \frac{dB(\omega)}{d\omega} d\omega \approx m_k^{(\text{Chebyshev})} = \Omega_b^k \sum_{n=0}^{2N_{\rm it}} \mu_n I_n^{(k)}, \tag{83}$$

with integrals $I_n^{(k)}$ defined as:

$$I_n^{(k)} = \frac{2}{\pi} \int_0^1 x^k \frac{T_n(x)}{\sqrt{1-x^2}} dx. \tag{84}$$

For $x \in [-1, +1]$ and even $k \in \mathbb{N}_0$, the following expression holds:

$$x^k = \frac{1}{2^{k-1}} \sum_{j=0}^{k/2} \frac{1}{1+\delta_{j,0}} \binom{k}{\frac{k}{2}-j} T_j(x). \tag{85}$$

Combined with the identity:

$$2T_m(x)T_n(x) = T_{m+n}(x) + T_{|m-n|}(x), \tag{86}$$

one can easily calculate:

$$I_n^{(k)} = \sum_{j=0}^{k/2} \frac{1}{1+\delta_{j,0}} \frac{1}{2^k} \binom{k}{\frac{k}{2}-j} + \\ + \left(\operatorname{sinc}\left(\frac{\pi}{2}(n+j)\right) + \operatorname{sinc}\left(\frac{\pi}{2}|n-j|\right)\right), \tag{87}$$

where $\operatorname{sinc}(x) = \sin x/x$. If we precalculate and store the integrals $I_n^{(k)}$, the moment $m_k^{(\text{Chebyshev})}$ for even $k \geq 0$ is, according to Eq. (83), given by a simple scalar product of the $(\mu_n)_{n=0}^{2N_{\text{it}}}$ coefficients with the integrals $\left(I_n^{(k)}\right)_{n=0}^{2N_{\text{it}}}$. In the case of even but negative values of k, we cannot follow the same procedure of integrating term-by-term in Eq. (83) because for negative k, the integrals $I_n^{(k)}$ diverge in general. Therefore, because we have the response function evaluated on Chebyshev frequency nodes:

$$\left(\frac{dB(\omega_i)}{d\omega}\right)_{i=1}^{N_e}, \quad \left(\omega_i = \Omega_b \cos\left(\frac{\pi}{N_e}\left(i-\frac{1}{2}\right)\right)\right)_{i=1}^{N_e}, \tag{88}$$

we can try using the Gauss-Chebyshev integration formula:

$$\int_0^1 f(x)dx \approx \frac{\pi}{n} \sum_{i=\left\lceil \frac{n+1}{2}\right\rceil}^{n} f(x_i)\sqrt{1-x_i^2}, \quad x_i = \cos\left(\frac{\pi}{n}\left(i-\frac{1}{2}\right)\right), \tag{89}$$

and obtain an approximate value of the moment m_k:

$$m_k \approx \frac{\pi}{N_e} \sum_{i=\left\lceil \frac{N_e+1}{2}\right\rceil}^{N_e} \omega_i^k \frac{dB(\omega_i)}{d\omega}\sqrt{\Omega_b^2-\omega_i^2}. \tag{90}$$

However, it turns out that this approximation is poor and the method is not suited for calculating the moments with $k < 0$ due to the ω^k factor that appears in the integrand of Eq. (77).

In order to test the method for even $k \geq 0$, we have again generated synthetic QRPA matrices A and B and vectors F^{20} and F^{02}, as in Sec. 4.1. After experimenting with various kernels, we have found that for the $k = 0$ moment, the best results (in a sense of convergence speed with increasing N_{it}) are obtained with Jackson kernel, while for other even $k > 0$ moments, Dirichlet kernel yields fastest convergence. In Fig. 13 we display the difference between the true value of the moment m_k, for even $k \geq 0$, and the value calculated by using the KPM as a function of the number of iterations N_{it}. We notice that convergence rate increases with k and for the $k = 0$ moment m_0 the convergence rate is very slow. This behavior can easily be explained by the structure of the response function Eq. (65). The delta functions $\delta(\omega \pm \Omega_i)$ are smeared when approximated by the Chebyshev series and by increasing the number of iterations N_{it} they become more narrow. For instance, if Lorentz kernel is used, the smearing is given by γ_{KPM} in Eq. (68). For small QRPA eigenfrequencies and insufficient number of iterations (i.e. too large smearing), approximations of delta functions are smeared outside the integration interval Eq. (77). This problem is less pronounced for $k > 0$ because the ω^k factor reduces the value of the integrand for small values of ω. Hence, the convergence will be faster for larger k values and very slow for $k = 0$, in accordance with results shown in Fig. 13.

We have also verified that moments are calculated correctly if realistic RPA matrices A and B and vectors F^{20}, F^{02}, generated by the `skyrme_rpa` code, are used.

In this section we have shown how to efficiently calculate the moments of the response function m_k for $k \geq -1$. We notice that we could generalize our approach, e.g. to calculate the integrals that include product of the Fermi integral function $f_{FI}(E)$ and the response function, appearing in the beta-decay rates formulas:

$$\lambda = \frac{\ln 2}{\kappa} \int_0^{+\infty} f_{FI}(\omega)\frac{dB(\omega)}{d\omega}d\omega = \frac{\ln 2}{\kappa}\sum_{i=1}^{N_p} f_{FI}(\Omega_i)|\langle i|\hat{F}|0\rangle|^2. \tag{91}$$

The only difference is that instead of the integrals $I_n^{(k)}$ in Eq. (84), we would calculate:

$$\frac{2}{\pi}\int_0^1 f_{FI}\left(\Omega_b x\right)\frac{T_n(x)}{\sqrt{1-x^2}}dx. \tag{92}$$

Because the Fermi integral function $f_{FI}(E)$ in the low-energy region is relatively small, we expect fast convergence in the same way we obtained fast convergence for even $k > 0$ moments. Approach using the contour integration of the QFAM strength function has already been applied on beta-decay rates calculations [36] and it would be interesting to compare the efficiency of the two approaches on realistic examples.

5. Summary and outlook

In this paper we have proposed an implementation of the kernel polynomial method, already successfully employed in the solid state physics [21,20], adapted for efficient calculation of the QRPA response function. The method is based on the expansion of the QRPA response function in an orthonormal basis of Chebyshev polynomials thus reducing the problem to the evaluation of the expansion coefficients. In practical calculations the expansion has to be truncated and because the QRPA response function is essentially a sum of weighted delta functions one encounters the problem of Gibbs oscillations. Standard procedure to damp the Gibbs oscillations and improve the precision of the Chebyshev series expansion is to convolute the response function with various damping kernels, e.g. Jackson or Lorentz kernel.

The proposed implementation of the KPM has been benchmarked and tested by comparing the QRPA response function with the one calculated by direct diagonalization of the QRPA matrices or by solving the QFAM equations. Our results demonstrate that the KPM can reproduce the QRPA and QFAM results to a high numerical accuracy. However, the efficiency of implementing the KPM depends significantly on the range of the eigenvalues of the QRPA matrix, i.e., broad range of eigenvalues requires a large number of iterations within the KPM implementation. In the following, we list the main advantages and drawbacks of implementing the KPM in calculating the QRPA response function.

Advantages of the KPM include:

- The KPM provides the response function on the entire frequency interval $\langle -\Omega_b, +\Omega_b\rangle$[4] compared to QFAM which calculates the response for a discrete set of frequencies.
- If one performs QFAM calculation with very small value of smearing width γ and frequency ω close to the pole, the linear system (10) is ill-conditioned requiring a large number of iterations to be solved, e.g. by the Broyden method which is often used for that purpose in QFAM solvers. The proposed implementation of the KPM circumvents this problem.

[4] Once we calculate the coefficients in the Chebyshev expansion, we can easily evaluate the approximation of the response function for any given frequency.

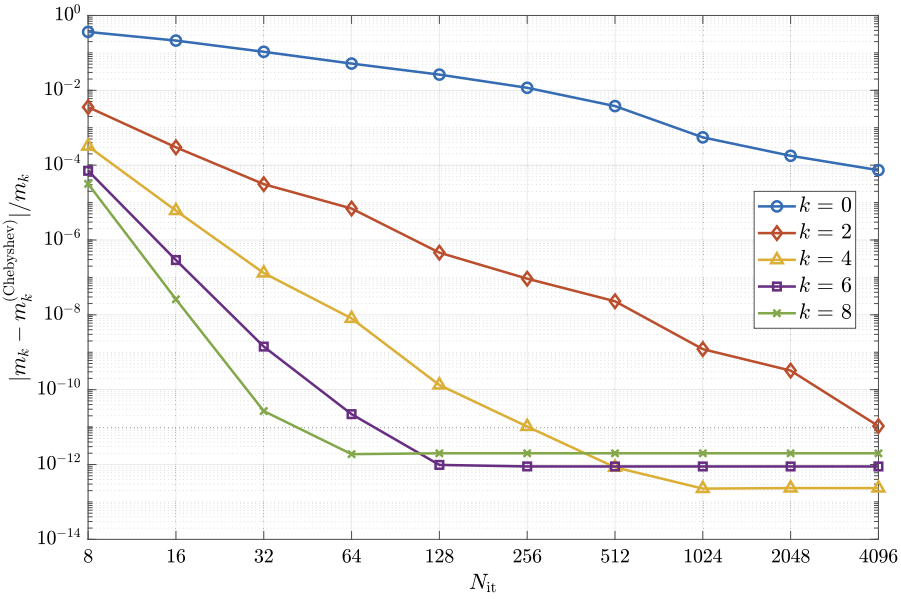

Fig. 13. (Color online) Convergence of even $k \geq 0$ moments as number of iterations N_{it} is increased. For $k = 0$ moment, Jackson kernel is used, while for $k > 0$ moments, Dirichlet kernel is used. Notice the logarithmic scales.

- The KPM can be implemented into any available QFAM solver with minimum programming effort.
- If the bounding frequency Ω_b is small, i.e. if the eigenfrequencies Ω_i are bounded in a relatively small interval, the method can locate the QRPA poles with large transition strength much quicker in comparison to the QFAM approach which can be crucial for many applications.
- The resolution of the standard QFAM calculation is determined by the smearing γ, i.e., in order to increase the resolution of the response one has to repeat the entire calculation with smaller value of γ. On the contrary, the Chebyshev KPM approach requires only larger number of iterations N_{it} to obtain a response function with better resolution in terms of smearing γ_{KPM} and there is no need to repeat the entire calculation.

Drawbacks of the KPM include:

- Appearance of the Gibbs oscillations. This problem can be addressed by introducing damping kernel, e.g. Lorentz kernel. The damping is controlled by the λ parameter in Eq. (53) with large values (e.g. $\lambda \approx 5$) leading to negligible effects of the Gibbs oscillations. However, according to Eq. (68), increasing the value of the λ parameter requires larger number of iterations N_{it} in order to obtain targeted resolution γ_{KPM}. Hence, one has to choose a value of the λ parameter that presents a satisfactory compromise between sufficient damping of Gibbs oscillations and convergence speed in terms of resolution γ_{KPM}.
- If the poles of the response function Ω_i are distributed across large energy region, i.e. if the bounding frequency Ω_b has to be relatively large in order to include all the poles in the interval $\langle -\Omega_b, +\Omega_b \rangle$, the KPM requires a large number of iterations N_{it} in order to produce a satisfactory resolution γ_{KPM}.
- The KPM cannot be used to calculate the response function in a localized energy region of interest (e.g. low-energy region up to 20 MeV), but rather globally on the entire $\langle -\Omega_b, +\Omega_b \rangle$ interval.
- The KPM can not be parallelized since recursion (45) operates sequentially. On the contrary, QFAM calculation can be easily parallelized because the response for each frequency is calculated independently.
- The KPM calculation diverges in the presence of the imaginary QRPA eigenfrequency, thus it should be applied only if the ground state corresponds to the HFB minimum.

Overall, the KPM is better suited for models based on the nonrelativistic EDFs [37,17,38,39] because in models based on relativistic EDFs the appearance of the Dirac sea necessitates large values of the bounding frequency. When applied to the models based on the nonrelativistic EDFs, we believe that the method can significantly speed up the process of finding the response function with high resolution in terms of smearing.

Declaration of competing interest

The authors declare that they have no known competing financial interests or personal relationships that could have appeared to influence the work reported in this paper.

Data availability

All data and codes are available at the public Github repository (see Ref. 27 in the manuscript).

Acknowledgements

This work has been supported by the Croatian Science Foundation under the projects Uncertainty quantification within the nuclear energy density functional framework (IP-2018-01-5987) and Randomized low rank algorithms and applications to parameter dependent problems (IP-2019-04-6268). It has also been supported by the QuantiXLie Centre of Excellence, a project co-financed by the Croatian Government and European Union through the European Regional Development Fund - the Competitiveness and Cohesion Operational Programme (KK.01.1.1.01.0004).

Appendix A. Existence of the QRPA eigenvalue problem solution

In this Appendix, we rigorously prove that in the case of positive-definite QRPA matrix, there exist positive eigenfrequencies $\Omega_i > 0$ and QRPA amplitudes X^i, Y^i, which are the generalized

eigenpair of the QRPA matrix (16) satisfying the generalized normalization and closure relations (17). We start with two lemmas which describe the structure of eigenvectors of the QRPA and HFB matrices followed by a proposition covering the result. Much more detailed treatment of general QRPA eigenproblem can be found in Refs. [7,8,40,41], however for convenience we provide here an easy to follow proof.

Lemma 4. *Let $A, B \in \mathbb{C}^{n\times n}$ such that $A^\dagger = A$ and $B^T = B$. Then there exist $Q \in \mathbb{C}^{n\times 2n}$ and diagonal $\mathrm{diag}[D_i]_{i=1}^{2n} \in \mathbb{R}^{2n\times 2n}$ such that $\begin{bmatrix} Q \\ Q^* \end{bmatrix} \in \mathbb{C}^{2n\times 2n}$ is unitary and:*

$$\begin{bmatrix} A & B \\ B^* & A^* \end{bmatrix} = \begin{bmatrix} Q \\ Q^* \end{bmatrix} \mathrm{diag}[D_i]_{i=1}^{2n} \begin{bmatrix} Q \\ Q^* \end{bmatrix}^\dagger. \tag{A.1}$$

Proof. Let us denote a Hermitian matrix $\mathcal{S} := \begin{bmatrix} A & B \\ B^* & A^* \end{bmatrix} \in \mathbb{C}^{2n\times 2n}$. Notice that for an eigenvalue $D \in \mathbb{R}$, if $\begin{bmatrix} x \\ y \end{bmatrix} \in \mathrm{Ker}\,(\mathcal{S} - D\mathbf{I}_{2n\times 2n})$, then also $\begin{bmatrix} y^* \\ x^* \end{bmatrix} \in \mathrm{Ker}\,(\mathcal{S} - D\mathbf{I}_{2n\times 2n})$. Let us fix an eigenvalue $D \in \sigma(\mathcal{S}) \subset \mathbb{R}$ with eigenspace $V_D := \mathrm{Ker}\,(\mathcal{S} - D\mathbf{I}_{2n\times 2n})$, and suppose $\dim V_D = p \in \mathbb{N}$. We will show that there exist orthonormal set of vectors: $\begin{bmatrix} x_1 \\ x_1^* \end{bmatrix}, \ldots, \begin{bmatrix} x_p \\ x_p^* \end{bmatrix} \in \mathbb{C}^{2n}$, such that: $\mathrm{span}\left\{\begin{bmatrix} x_1 \\ x_1^* \end{bmatrix}, \ldots, \begin{bmatrix} x_p \\ x_p^* \end{bmatrix}\right\} = V_D$. Suppose we have $0 \le l < p$ orthonormal vectors: $\begin{bmatrix} x_1 \\ x_1^* \end{bmatrix}, \ldots, \begin{bmatrix} x_l \\ x_l^* \end{bmatrix} \in V_D$. We will show how to construct a normalized vector $\begin{bmatrix} x_{l+1} \\ x_{l+1}^* \end{bmatrix} \in V_D$, which is orthogonal to previous vectors: $\begin{bmatrix} x_{l+1} \\ x_{l+1}^* \end{bmatrix} \perp \begin{bmatrix} x_1 \\ x_1^* \end{bmatrix}, \ldots, \begin{bmatrix} x_l \\ x_l^* \end{bmatrix}$. Since $l < p$, there exists $\begin{bmatrix} x \\ y \end{bmatrix} \in V_D$ such that $\begin{bmatrix} x \\ y \end{bmatrix} \notin \mathrm{span}\left\{\begin{bmatrix} x_1 \\ x_1^* \end{bmatrix}, \ldots, \begin{bmatrix} x_l \\ x_l^* \end{bmatrix}\right\}$. We can easily orthogonalize $\begin{bmatrix} x \\ y \end{bmatrix}$ against other vectors $\left\{\begin{bmatrix} x_1 \\ x_1^* \end{bmatrix}, \ldots, \begin{bmatrix} x_l \\ x_l^* \end{bmatrix}\right\}$, i.e. there exists a normalized vector $\begin{bmatrix} x \\ y \end{bmatrix} \in V_D$, such that $\begin{bmatrix} x \\ y \end{bmatrix} \perp \begin{bmatrix} x_1 \\ x_1^* \end{bmatrix}, \ldots, \begin{bmatrix} x_l \\ x_l^* \end{bmatrix}$. This gives a normalized vector $\begin{bmatrix} y^* \\ x^* \end{bmatrix} \in V_D$, such that:

$$\left\langle \begin{bmatrix} y^* \\ x^* \end{bmatrix}, \begin{bmatrix} x_i \\ x_i^* \end{bmatrix} \right\rangle = \left\langle \begin{bmatrix} x \\ y \end{bmatrix}, \begin{bmatrix} x_i \\ x_i^* \end{bmatrix} \right\rangle^* = 0, \ \forall i = 1, \ldots, l. \tag{A.2}$$

Thus, there exist two normalized vectors $\begin{bmatrix} x \\ y \end{bmatrix}, \begin{bmatrix} y^* \\ x^* \end{bmatrix} \in V_D$, orthogonal to previous vectors: $\begin{bmatrix} x \\ y \end{bmatrix}, \begin{bmatrix} y^* \\ x^* \end{bmatrix} \perp \begin{bmatrix} x_1 \\ x_1^* \end{bmatrix}, \ldots, \begin{bmatrix} x_l \\ x_l^* \end{bmatrix}$. We differentiate two cases:

1. Assume that $y = -x^*$. Define $z := \mathrm{i}x \in \mathbb{C}^n$. Then $\begin{bmatrix} z \\ z^* \end{bmatrix} = \mathrm{i}\begin{bmatrix} x \\ y \end{bmatrix}$, and thus we constructed a normalized vector $\begin{bmatrix} z \\ z^* \end{bmatrix} \in V_D$, orthogonal to previous vectors: $\begin{bmatrix} z \\ z^* \end{bmatrix} \perp \begin{bmatrix} x_1 \\ x_1^* \end{bmatrix}, \ldots, \begin{bmatrix} x_l \\ x_l^* \end{bmatrix}$.
2. Assume that $y \neq -x^*$, i.e. $x + y^* \neq \mathbf{0}_n$. Define $z := \frac{1}{\sqrt{2}||x+y^*||}(x + y^*) \in \mathbb{C}^n$. Then $\begin{bmatrix} z \\ z^* \end{bmatrix} = \frac{1}{\sqrt{2}||x+y^*||}\left(\begin{bmatrix} x \\ y \end{bmatrix} + \begin{bmatrix} y^* \\ x^* \end{bmatrix}\right) \in V_D$ is a normalized vector orthogonal to previous vectors: $\begin{bmatrix} z \\ z^* \end{bmatrix} \perp \begin{bmatrix} x_1 \\ x_1^* \end{bmatrix}, \ldots, \begin{bmatrix} x_l \\ x_l^* \end{bmatrix}$.

Thus, we constructed a normalized vector $\begin{bmatrix} x_{l+1} \\ x_{l+1}^* \end{bmatrix} \in V_D$ orthogonal to previous vectors $\begin{bmatrix} x_{l+1} \\ x_{l+1}^* \end{bmatrix} \perp \begin{bmatrix} x_1 \\ x_1^* \end{bmatrix}, \ldots, \begin{bmatrix} x_l \\ x_l^* \end{bmatrix}$. Repeating this procedure $p = \dim V_D$ times, we obtain an orthonormal basis for the eigenspace $V_D = \mathrm{span}\left\{\begin{bmatrix} x_1 \\ x_1^* \end{bmatrix}, \ldots, \begin{bmatrix} x_p \\ x_p^* \end{bmatrix}\right\}$. Therefore, there exists $\boldsymbol{x}_D \in \mathbb{C}^{n\times \dim V_D}$ such that the matrix $\begin{bmatrix} \boldsymbol{x}_D \\ \boldsymbol{x}_D^* \end{bmatrix} \in \mathbb{C}^{2n\times \dim V_D}$ has orthonormal column vectors and $\mathcal{S}\begin{bmatrix} \boldsymbol{x}_D \\ \boldsymbol{x}_D^* \end{bmatrix} = D\begin{bmatrix} \boldsymbol{x}_D \\ \boldsymbol{x}_D^* \end{bmatrix}$. Repeating this argument for each eigenvalue $D \in \sigma(\mathcal{S})$ having degeneracy $\dim V_D$, and using the fact that two eigenvectors of Hermitian matrix that correspond to two different eigenvalues are orthogonal, we obtain a matrix $Q \in \mathbb{C}^{n\times 2n}$ such that $\begin{bmatrix} Q \\ Q^* \end{bmatrix} \in \mathbb{C}^{2n\times 2n}$ is unitary and $\mathcal{S}\begin{bmatrix} Q \\ Q^* \end{bmatrix} = \begin{bmatrix} Q \\ Q^* \end{bmatrix} \mathrm{diag}[D]_{D\in\sigma(\mathcal{S})}$. □

Lemma 5. *Let $h, \Delta \in \mathbb{C}^{n\times n}$ such that $h^\dagger = h$ and $\Delta^T = -\Delta$ with $\begin{bmatrix} h & \Delta \\ -\Delta^* & -h^* \end{bmatrix} \in \mathbb{C}^{2n\times 2n}$ invertible. Then there exist $U, V \in \mathbb{C}^{n\times n}$ and diagonal $E \in \mathbb{R}^{n\times n}$ with positive diagonal elements such that $\begin{bmatrix} U & V^* \\ V & U^* \end{bmatrix} \in \mathbb{C}^{2n\times 2n}$ is unitary and:*

$$\begin{bmatrix} h & \Delta \\ -\Delta^* & -h^* \end{bmatrix} = \begin{bmatrix} U & V^* \\ V & U^* \end{bmatrix} \begin{bmatrix} +E & \mathbf{0} \\ \mathbf{0} & -E \end{bmatrix} \begin{bmatrix} U & V^* \\ V & U^* \end{bmatrix}^\dagger. \tag{A.3}$$

Proof. The proof can be found in Ref. [8]. □

Proposition 1. *Let $A, B \in \mathbb{C}^{n\times n}$ such that $A^\dagger = A$, $B^T = B$ and $\begin{bmatrix} A & B \\ B^* & A^* \end{bmatrix} \in \mathbb{C}^{2n\times 2n}$ is positive-definite. Then there exist $X, Y \in \mathbb{C}^{n\times n}$ and diagonal $\Omega \in \mathbb{R}^{n\times n}$ with positive diagonal elements such that there holds:*

$$\begin{bmatrix} A & B \\ B^* & A^* \end{bmatrix} \begin{bmatrix} X & Y^* \\ Y & X^* \end{bmatrix} = \begin{bmatrix} \mathbf{I} & \mathbf{0} \\ \mathbf{0} & -\mathbf{I} \end{bmatrix} \begin{bmatrix} X & Y^* \\ Y & X^* \end{bmatrix} \begin{bmatrix} +\Omega & \mathbf{0} \\ \mathbf{0} & -\Omega \end{bmatrix}, \tag{A.4}$$

and:

$$\begin{bmatrix} X & Y^* \\ Y & X^* \end{bmatrix} \begin{bmatrix} \mathbf{I} & \mathbf{0} \\ \mathbf{0} & -\mathbf{I} \end{bmatrix} \begin{bmatrix} X & Y^* \\ Y & X^* \end{bmatrix}^\dagger = \begin{bmatrix} \mathbf{I} & \mathbf{0} \\ \mathbf{0} & -\mathbf{I} \end{bmatrix}. \tag{A.5}$$

Proof. Due to the Lemma 4 and positive-definiteness of $\begin{bmatrix} A & B \\ B^* & A^* \end{bmatrix}$, there exist unitary $\begin{bmatrix} q_1 & q_2 \\ q_1^* & q_2^* \end{bmatrix} \in \mathbb{C}^{2n\times 2n}$ for $q_1, q_2 \in \mathbb{C}^{n\times n}$ and diagonal $d_1, d_2 \in \mathbb{R}^{n\times n}$ with positive diagonal elements such that:

$$\begin{bmatrix} A & B \\ B^* & A^* \end{bmatrix} = \begin{bmatrix} q_1 & q_2 \\ q_1^* & q_2^* \end{bmatrix} \begin{bmatrix} d_1 & \mathbf{0} \\ \mathbf{0} & d_2 \end{bmatrix} \begin{bmatrix} q_1 & q_2 \\ q_1^* & q_2^* \end{bmatrix}^\dagger. \tag{A.6}$$

Then, a square root matrix $\begin{bmatrix} A & B \\ B^* & A^* \end{bmatrix}^{1/2}$ is well defined as:

$$\begin{bmatrix} A & B \\ B^* & A^* \end{bmatrix}^{1/2} := \begin{bmatrix} q_1 & q_2 \\ q_1^* & q_2^* \end{bmatrix} \begin{bmatrix} \sqrt{d_1} & \mathbf{0} \\ \mathbf{0} & \sqrt{d_2} \end{bmatrix} \begin{bmatrix} q_1 & q_2 \\ q_1^* & q_2^* \end{bmatrix}^\dagger. \tag{A.7}$$

Trivial calculation shows that the invertible matrix:

$$\begin{bmatrix} A & B \\ B^* & A^* \end{bmatrix}^{1/2} \begin{bmatrix} \mathbf{I} & \mathbf{0} \\ \mathbf{0} & -\mathbf{I} \end{bmatrix} \begin{bmatrix} A & B \\ B^* & A^* \end{bmatrix}^{1/2}, \tag{A.8}$$

has the same structure as the HFB matrix in Lemma 5. Therefore, according to Lemma 5, there exist unitary $\begin{bmatrix} x & y^* \\ y & x^* \end{bmatrix} \in \mathbb{C}^{2n\times 2n}$ and diagonal $\Omega \in \mathbb{R}^{n\times n}$ with positive diagonal elements, such that:

$$\begin{bmatrix} A & B \\ B^* & A^* \end{bmatrix}^{1/2} \begin{bmatrix} \mathbf{I} & \mathbf{0} \\ \mathbf{0} & -\mathbf{I} \end{bmatrix} \begin{bmatrix} A & B \\ B^* & A^* \end{bmatrix}^{1/2} = \begin{bmatrix} x & y^* \\ y & x^* \end{bmatrix} \begin{bmatrix} +\Omega & \mathbf{0} \\ \mathbf{0} & -\Omega \end{bmatrix} \begin{bmatrix} x & y^* \\ y & x^* \end{bmatrix}^\dagger. \tag{A.9}$$

Let us define matrices $X, Y \in \mathbb{C}^{n\times n}$ as:

$$\begin{bmatrix} X & Y^* \\ Y & X^* \end{bmatrix} := \begin{bmatrix} \mathbf{I} & \mathbf{0} \\ \mathbf{0} & -\mathbf{I} \end{bmatrix} \begin{bmatrix} A & B \\ B^* & A^* \end{bmatrix}^{1/2} \times \times \begin{bmatrix} x & y^* \\ y & x^* \end{bmatrix} \begin{bmatrix} +\Omega^{-1/2} & \mathbf{0} \\ \mathbf{0} & -\Omega^{-1/2} \end{bmatrix}. \tag{A.10}$$

Notice that the matrix on the right-hand side in Eq. (A.10) indeed has the structure as the one on the left-hand side, i.e. matrices X and Y are well defined. Straightforward calculation then gives:

$$\begin{bmatrix} A & B \\ B^* & A^* \end{bmatrix} \begin{bmatrix} X & Y^* \\ Y & X^* \end{bmatrix} = \begin{bmatrix} \mathbf{I} & \mathbf{0} \\ \mathbf{0} & -\mathbf{I} \end{bmatrix} \begin{bmatrix} X & Y^* \\ Y & X^* \end{bmatrix} \begin{bmatrix} +\Omega & \mathbf{0} \\ \mathbf{0} & -\Omega \end{bmatrix}, \tag{A.11}$$

and:

$$\begin{bmatrix} X & Y^* \\ Y & X^* \end{bmatrix}^\dagger \begin{bmatrix} \mathbf{I} & \mathbf{0} \\ \mathbf{0} & -\mathbf{I} \end{bmatrix} \begin{bmatrix} X & Y^* \\ Y & X^* \end{bmatrix} = \begin{bmatrix} \mathbf{I} & \mathbf{0} \\ \mathbf{0} & -\mathbf{I} \end{bmatrix}. \tag{A.12}$$

Previous equation shows that:

$$\begin{bmatrix} X & Y^* \\ Y & X^* \end{bmatrix}^{-1} = \begin{bmatrix} \mathbf{I} & \mathbf{0} \\ \mathbf{0} & -\mathbf{I} \end{bmatrix} \begin{bmatrix} X & Y^* \\ Y & X^* \end{bmatrix}^\dagger \begin{bmatrix} \mathbf{I} & \mathbf{0} \\ \mathbf{0} & -\mathbf{I} \end{bmatrix}, \tag{A.13}$$

which finally gives:

$$\begin{bmatrix} X & Y^* \\ Y & X^* \end{bmatrix} \begin{bmatrix} \mathbf{I} & \mathbf{0} \\ \mathbf{0} & -\mathbf{I} \end{bmatrix} \begin{bmatrix} X & Y^* \\ Y & X^* \end{bmatrix}^\dagger = \begin{bmatrix} \mathbf{I} & \mathbf{0} \\ \mathbf{0} & -\mathbf{I} \end{bmatrix}. \quad \square \tag{A.14}$$

Appendix B. Synthetic generation of the QRPA matrices

In this Appendix we present some mathematical results that can be useful for synthetic generation of matrices involved in the QRPA equation. Such synthetic matrices can be used for numerical experiments and various tests. First, we prove the Bloch-Messiah theorem for bosons stated in Appendix E of Ref. [7], and then give a Remark explaining a procedure for generating QRPA matrix. In the literature, we could not find a detailed and easy to follow proof of the Bloch-Messiah theorem for bosons, and for completeness we provide a detailed proof here.

Theorem 1. *Let $X, Y \in \mathbb{C}^{n\times n}$ such that they satisfy:*

$$\begin{bmatrix} X & Y^* \\ Y & X^* \end{bmatrix} \begin{bmatrix} \mathbf{I} & \mathbf{0} \\ \mathbf{0} & -\mathbf{I} \end{bmatrix} \begin{bmatrix} X & Y^* \\ Y & X^* \end{bmatrix}^\dagger = \begin{bmatrix} \mathbf{I} & \mathbf{0} \\ \mathbf{0} & -\mathbf{I} \end{bmatrix}. \tag{B.1}$$

Then there exist unitary $C, D \in \mathbb{C}^{n\times n}$ and $\theta_1, \theta_2, \ldots, \theta_n \geq 0$ such that:

$$X = D \operatorname{diag}[\cosh\theta_i]_{i=1}^n C \quad \textit{and} \quad Y = D^* \operatorname{diag}[\sinh\theta_i]_{i=1}^n C. \tag{B.2}$$

Proof. The proof is similar to the proof of the Bloch-Messiah decomposition where in this case the role of the Youla decomposition of skew-symmetric matrix plays the Autonne-Takagi factorization of symmetric complex matrix. From equation:

$$\begin{bmatrix} X & Y^* \\ Y & X^* \end{bmatrix} \begin{bmatrix} \mathbf{I} & \mathbf{0} \\ \mathbf{0} & -\mathbf{I} \end{bmatrix} \begin{bmatrix} X & Y^* \\ Y & X^* \end{bmatrix}^\dagger = \begin{bmatrix} \mathbf{I} & \mathbf{0} \\ \mathbf{0} & -\mathbf{I} \end{bmatrix}, \tag{B.3}$$

one obtains: $\begin{bmatrix} X & Y^* \\ Y & X^* \end{bmatrix}^{-1} = \begin{bmatrix} \mathbf{I} & \mathbf{0} \\ \mathbf{0} & -\mathbf{I} \end{bmatrix} \begin{bmatrix} X & Y^* \\ Y & X^* \end{bmatrix}^\dagger \begin{bmatrix} \mathbf{I} & \mathbf{0} \\ \mathbf{0} & -\mathbf{I} \end{bmatrix}$, which gives:

$$\begin{bmatrix} X & Y^* \\ Y & X^* \end{bmatrix}^\dagger \begin{bmatrix} \mathbf{I} & \mathbf{0} \\ \mathbf{0} & -\mathbf{I} \end{bmatrix} \begin{bmatrix} X & Y^* \\ Y & X^* \end{bmatrix} = \begin{bmatrix} \mathbf{I} & \mathbf{0} \\ \mathbf{0} & -\mathbf{I} \end{bmatrix}. \tag{B.4}$$

Thus, the assumption of the Theorem gives $X, Y \in \mathbb{C}^{n\times n}$ which according to (B.3) and (B.4) satisfy:

$$XX^\dagger - Y^*Y^T = \mathbf{I}, \tag{B.5}$$

$$YX^\dagger = X^*Y^T, \tag{B.6}$$

$$X^\dagger X - Y^\dagger Y = \mathbf{I}, \tag{B.7}$$

$$Y^T X = X^T Y. \tag{B.8}$$

Let $X = U_x^\dagger \Sigma_x V_x$ be singular value decomposition of X, where $U_x, V_x \in \mathbb{C}^{n\times n}$ are unitary and $\Sigma_x = \operatorname{diag}[x_i]_{i=1}^n$ is diagonal matrix containing singular values: $(x_i)_{i=1}^n \subset [0, +\infty\rangle$. We will first show that all $(x_i)_{i=1}^n$ are positive. From (B.7) there holds: $Y^\dagger Y = V_x^\dagger(\Sigma_x^2 - \mathbf{I})V_x$, which gives $\sigma(Y^\dagger Y) = \{x_i^2 - 1 : i = 1, \ldots, n\}$. Since $Y^\dagger Y$ is Hermitian and positive-semidefinite, there holds $\sigma(Y^\dagger Y) \subset [0, +\infty\rangle$, which yields $x_i^2 - 1 \geq 0$, and thus $x_i \geq 1 > 0$, for all $i = 1, \ldots, n$. Define $\widetilde{X} := U_x X V_x^\dagger = \Sigma_x$ and $\widetilde{Y} := U_x^* Y V_x^\dagger$. One can easily show that $\widetilde{X}, \widetilde{Y} \in \mathbb{C}^{n\times n}$ also satisfy relations (B.5)-(B.8). Let us assume that the Theorem is true in the case if $X \in \mathbb{C}^{n\times n}$ is Hermitian and positive-definite. In that case, applying the Theorem on $\widetilde{X}, \widetilde{Y} \in \mathbb{C}^{n\times n}$, there exist $\widetilde{D}, \widetilde{C} \in \mathbb{C}^{n\times n}$ unitary and $\theta_1, \ldots, \theta_n \geq 0$, such that $\widetilde{X} = \widetilde{D} \operatorname{diag}[\cosh\theta_i]_{i=1}^n \widetilde{C}$ and $\widetilde{Y} = \widetilde{D}^* \operatorname{diag}[\sinh\theta_i]_{i=1}^n \widetilde{C}$, yielding finally: $X = D \operatorname{diag}[\cosh\theta_i]_{i=1}^n C$ and $Y = D^* \operatorname{diag}[\sinh\theta_i]_{i=1}^n C$, where $D = U_x^\dagger \widetilde{D}$ and $C = \widetilde{C} V_x$ are unitary matrices. Therefore, if we prove the Theorem with additional assumption that $X \in \mathbb{C}^{n\times n}$ is Hermitian and positive definite, the proof will be completed and thus assume that $X, Y \in \mathbb{C}^{n\times n}$ satisfy (B.5)-(B.8), where $X \in \mathbb{C}^{n\times n}$ is Hermitian and positive-definite matrix. Since X is Hermitian and positive-definite, its spectral decomposition is:

$$X = Z \left[\bigoplus_{i=1}^p x_i \mathbf{I}_{n_i \times n_i} \right] Z^\dagger, \tag{B.9}$$

where $Z \in \mathbb{C}^{n\times n}$ is unitary and $x_1^{[n_1]}, \ldots, x_p^{[n_p]} > 0$, are its eigenvalues having degeneracies: $n_1, \ldots, n_p \in \mathbb{N}$, with $n_1 + \cdots + n_p = n$. Define $\rho := XX^\dagger \in \mathbb{C}^{n\times n}$ and $\kappa := YX^\dagger \in \mathbb{C}^{n\times n}$. According to Eq. (B.6), $\kappa \in \mathbb{C}^{n\times n}$ satisfies: $\kappa = YX^\dagger = X^*Y^T$, thus giving: $\kappa^T = \kappa$. Multiplying Eq. (B.8) by $X^\dagger$ from the right and by X^* from the left yields:

$$\kappa\rho = \rho^*\kappa. \tag{B.10}$$

We have $\rho = XX^\dagger = Z\left[\bigoplus_{i=1}^n x_i^2 \mathbf{I}_{n_i\times n_i}\right] Z^\dagger$, which combined with (B.10) gives:

$$(Z^T\kappa Z)\left[\bigoplus_{i=1}^n x_i^2 \mathbf{I}_{n_i\times n_i}\right] = \left[\bigoplus_{i=1}^n x_i^2 \mathbf{I}_{n_i\times n_i}\right](Z^T\kappa Z). \tag{B.11}$$

Previous equation gives the equality for blocks in matrix $Z^T\kappa Z$:

$$(x_i^2 - x_j^2)(Z^T\kappa Z)_{[i,j]} = \mathbf{0}_{n_i\times n_j},\ i, j = 1, \ldots, p, \tag{B.12}$$

which because $x_1, \ldots, x_p > 0$ are positive gives:

$$(Z^T\kappa Z)_{[i,j]} = \mathbf{0}_{n_i\times n_j},\ i \neq j = 1, \ldots, p, \tag{B.13}$$

i.e. $Z^T\kappa Z$ is block diagonal matrix:

$$Z^T\kappa Z = \bigoplus_{i=1}^p \widetilde{\kappa}_i, \tag{B.14}$$

having diagonal blocks $\widetilde{\kappa}_i \in \mathbb{C}^{n_i\times n_i}$, which are symmetric: $\widetilde{\kappa}_i^T = \widetilde{\kappa}_i$, because $Z^T\kappa Z$ is symmetric. Every complex symmetric matrix $\widetilde{\kappa}_i \in \mathbb{C}^{n_i\times n_i}$ has Autonne-Takagi factorization:

$$\widetilde{\kappa}_i = u_i^* \operatorname{diag}[\sigma_j^{(i)}]_{j=1}^{n_i} u_i^\dagger,\ i = 1, \ldots, p, \tag{B.15}$$

where $u_i \in \mathbb{C}^{n_i \times n_i}$ are unitary and $\sigma_1^{(i)}, \ldots, \sigma_{n_i}^{(i)} \geq 0$. Using these decompositions, from Eq. (B.14) we obtain:

$$(ZU)^T \kappa (ZU) = \bigoplus_{i=1}^{p} \operatorname{diag}[\sigma_j^{(i)}]_{j=1}^{n_i}, \tag{B.16}$$

where $U := \bigoplus_{i=1}^{p} u_i \in \mathbb{C}^{n \times n}$ is unitary block diagonal matrix. On the other hand, from (B.9), writing $\mathbf{I}_{n_i \times n_i} = u_i u_i^\dagger$, there holds:

$$X = Z \left[\bigoplus_{i=1}^{p} x_i u_i u_i^\dagger \right] Z^\dagger = (ZU) \left[\bigoplus_{i=1}^{p} \operatorname{diag}[x_i]_{j=1}^{n_i} \right] (ZU)^\dagger. \tag{B.17}$$

Writing $\kappa = Y X^\dagger$, Eq. (B.16) gives:

$$\begin{aligned} \bigoplus_{i=1}^{p} \operatorname{diag}[\sigma_j^{(i)}]_{j=1}^{n_i} &= (ZU)^T Y X^\dagger (ZU) \\ &= (ZU)^T Y (ZU) \cdot \left((ZU)^\dagger X (ZU) \right)^\dagger, \end{aligned} \tag{B.18}$$

which after using Eq. (B.17) and positivity of $x_1, \ldots, x_p > 0$ yields:

$$(ZU)^T Y (ZU) = \bigoplus_{i=1}^{p} \operatorname{diag}[\sigma_j^{(i)} / x_i]_{j=1}^{n_i}. \tag{B.19}$$

Let us define a unitary matrix $Q := ZU \in \mathbb{C}^{n \times n}$, and real non-negative numbers: $(y_j^{(i)})_{j=1}^{n_i} := (\sigma_j^{(i)} / x_i)_{j=1}^{n_i} \subset [0, +\infty\rangle$, for $i = 1, \ldots, p$. Then (B.17) and (B.19) finally give:

$$\begin{aligned} X &= Q \left[\bigoplus_{i=1}^{p} \operatorname{diag}[x_i]_{j=1}^{n_i} \right] Q^\dagger \quad \text{and} \\ Y &= Q^* \left[\bigoplus_{i=1}^{p} \operatorname{diag}[y_j^{(i)}]_{j=1}^{n_i} \right] Q^\dagger. \end{aligned} \tag{B.20}$$

Inserting (B.20) into (B.7) we obtain:

$$x_i^2 - \left(y_j^{(i)} \right)^2 = 1, \; j = 1, \ldots, n_i, \; i = 1, \ldots, p, \tag{B.21}$$

which shows that there exist $\theta_1, \ldots, \theta_n \geq 0$, and $Q \in \mathbb{C}^{n \times n}$ unitary such that:

$$X = Q \operatorname{diag}[\cosh \theta_i]_{i=1}^{n} Q^\dagger \quad \text{and} \quad Y = Q^* \operatorname{diag}[\sinh \theta_i]_{i=1}^{n} Q^\dagger, \tag{B.22}$$

which completes the proof in a special case where $X \in \mathbb{C}^{n \times n}$ is Hermitian and positive-definite. □

Remark 1. Suppose we want to generate a positive-definite QRPA matrix $\begin{bmatrix} A & B \\ B^* & A^* \end{bmatrix} \in \mathbb{C}^{2n \times 2n}$ having preselected positive eigenfrequencies $(\Omega_i)_{i=1}^{n}$. First, guided by the Theorem 1, we generate unitary matrices $C, D \in \mathbb{C}^{n \times n}$ together with $\theta_1, \theta_2, \ldots, \theta_n \geq 0$, and define:

$$X = D \operatorname{diag}[\cosh \theta_i]_{i=1}^{n} C, \quad Y = D^* \operatorname{diag}[\sinh \theta_i]_{i=1}^{n} C. \tag{B.23}$$

Second, we define matrices:

$$A = +\left[X \Omega X^\dagger + \left(Y \Omega Y^\dagger \right)^* \right], \quad B = -\left[X \Omega Y^\dagger + \left(X \Omega Y^\dagger \right)^T \right], \tag{B.24}$$

which satisfy $A^\dagger = A$ and $B^T = B$, where $\Omega = \operatorname{diag}[\Omega_i]_{i=1}^{n} \in \mathbb{R}^{n \times n}$. Then, one can easily see that (A.4) and (A.5) are satisfied. Also, (A.4) and (A.5) imply:

$$\begin{aligned} \begin{bmatrix} A & B \\ B^* & A^* \end{bmatrix} = \begin{bmatrix} \mathbf{I} & \mathbf{0} \\ \mathbf{0} & -\mathbf{I} \end{bmatrix} \begin{bmatrix} X & Y^* \\ Y & X^* \end{bmatrix} \begin{bmatrix} +\Omega & \mathbf{0} \\ \mathbf{0} & +\Omega \end{bmatrix} \times \\ \times \begin{bmatrix} X & Y^* \\ Y & X^* \end{bmatrix}^\dagger \begin{bmatrix} \mathbf{I} & \mathbf{0} \\ \mathbf{0} & -\mathbf{I} \end{bmatrix}, \end{aligned} \tag{B.25}$$

which evidently shows that the generated QRPA matrix $\begin{bmatrix} A & B \\ B^* & A^* \end{bmatrix}$ is positive-definite.

References

[1] M. Bender, P.-H. Heenen, P.-G. Reinhard, Rev. Mod. Phys. 75 (2003) 121.
[2] D. Vretenar, A.V. Afanasjev, G.A. Lalazissis, P. Ring, Phys. Rep. 409 (2005) 101.
[3] J.R. Stone, P.-G. Reinhard, Prog. Part. Nucl. Phys. 58 (2007) 587.
[4] T. Nikšić, D. Vretenar, P. Ring, Prog. Part. Nucl. Phys. 66 (2011) 519.
[5] N. Paar, D. Vretenar, E. Khan, G. Colo, Rep. Prog. Phys. 70 (2007) 691.
[6] D. Savran, T. Aumann, A. Zilges, Prog. Part. Nucl. Phys. 70 (2013) 210.
[7] P. Ring, P. Schuck, The Nuclear Many-Body Problem, Springer-Verlag, Berlin, 1980.
[8] J.-P. Blaizot, G. Ripka, Quantum Theory of Finite Systems, MIT, Cambridge, MA, 1986.
[9] T. Nakatsukasa, T. Inakura, K. Yabana, Phys. Rev. C 76 (2007) 024318.
[10] T. Inakura, T. Nakatsukasa, K. Yabana, Phys. Rev. C 80 (2009) 044301.
[11] T. Inakura, T. Nakatsukasa, K. Yabana, Phys. Rev. C 84 (2011) 021302.
[12] P. Avogadro, T. Nakatsukasa, Phys. Rev. C 84 (2011) 014314.
[13] M. Stoitsov, M. Kortelainen, T. Nakatsukasa, C. Losa, W. Nazarewicz, Phys. Rev. C 84 (2011) 041305(R).
[14] N. Hinohara, M. Korelainen, W. Nazarewicz, Phys. Rev. C 87 (2013) 064309.
[15] H. Liang, T. Nakatsukasa, Z. Niu, J. Meng, Phys. Rev. C 87 (2013) 054310.
[16] T. Nikšić, N. Kralj, T. Tutiš, D. Vretenar, P. Ring, Phys. Rev. C 88 (2013) 044327.
[17] M. Kortelainen, N. Hinohara, W. Nazarewicz, Phys. Rev. C 92 (2015) 051302.
[18] N. Hinohara, M. Kortelainen, W. Nazarewicz, E. Olse, Phys. Rev. C 91 (2015) 044323.
[19] X. Sun, D. Lu, Phys. Rev. C 96 (2017) 024614.
[20] A. Weisse, G. Wellein, A. Alvermann, H. Fehske, Rev. Mod. Phys. 78 (2006) 275.
[21] L. Covaci, F.M. Peeters, M. Berciu, Phys. Rev. Lett. 105 (2010) 167006.
[22] J.E. Sobczyk, A. Roggero, arXiv:2110.02108, 2021.
[23] J. Toivanen, B.G. Carlsson, J. Dobaczewski, K. Mizuyama, R.R. Rodríguez-Guzmán, P. Toivanen, P. Veselý, Phys. Rev. C 81 (2010) 034312.
[24] S. Péru, H. Goutte, Phys. Rev. C 77 (2008) 044313.
[25] C.W. Clenshaw, Math. Comput. 9 (1955) 118–120.
[26] FFTW Fast Fourier Transform Library, http://www.fftw.org/.
[27] https://github.com/abjelcic/ChebyshevQRPA.
[28] G. Colò, L. Cao, N. Van Giai, L. Capelli, Comput. Phys. Commun. 184 (2013) 142–161.
[29] E. Chabanat, P. Bonche, P. Hanesel, J. Meyer, R. Schaeffer, Nucl. Phys. A 627 (1997) 710.
[30] A. Bjelčić, T. Nikšić, Comput. Phys. Commun. 253 (2020) 107184.
[31] T. Nikšić, D. Vretenar, P. Ring, Phys. Rev. C 78 (2008) 034318.
[32] Y. Tian, Z.Y. Ma, P. Ring, Phys. Lett. B 676 (2009) 44.
[33] F. Dawson, R.J. Furnstahl, Phys. Rev. C 42 (1990) 2009.
[34] N. Hinohara, Phys. Rev. C 92 (2015) 034321.
[35] L. Capelli, G. Colò, J. Li, Phys. Rev. C 79 (2009) 054329.
[36] M.T. Mustonen, T. Shafer, Z. Zenginerler, J. Engel, Phys. Rev. C 90 (2014) 024308.
[37] M. Stoitsov, M. Kortelainen, T. Nakatsukasa, C. Losa, W. Nazarewicz, Phys. Rev. C 84 (2011) 041305.
[38] J.C. Pei, M. Kortelainen, Y.N. Zhang, F.R. Xu, Phys. Rev. C 90 (2014) 051304.
[39] K. Washiyama, T. Nakatsukasa, Phys. Rev. C 96 (2017) 041304.
[40] H. Nakada, Prog. Theor. Exp. Phys. 2016 (2016) 063D02.
[41] H. Nakada, Prog. Theor. Exp. Phys. 2017 (2017) 023D03.